Published in final edited form as:
Dev Biol. 2012 February 1; 362(1): 24–41. doi:10.1016/j.ydbio.2011.10.033.

Conditional Hypoxia Inducible Factor-1α Induction in Embryonic Pulmonary Epithelium Impairs Maturation and Augments Lymphangiogenesis

James P. Bridges[1,2], **Sui Lin**[1], **Machiko Ikegami**[1], and **John M. Shannon**[1]
[1]Perinatal Institute, Division of Pulmonary Biology, Cincinnati Children's Hospital Medical Center, Cincinnati, OH, USA

Abstract

Hypoxia inducible factor (HIF) 1a, EPAS1 and NEPAS are expressed in the embryonic mouse lung and each isoform exhibits distinct spatiotemporal expression patterns throughout morphogenesis. To further assess the role of the HIF1a isoform in lung epithelial cell differentiation and homeostasis, we created transgenic mice that express a constitutively active isoform of human HIF-1a (HIF-1a three point mutant (TPM)), in a doxycycline-dependent manner. Expression of HIF1a TPM in the developing pulmonary epithelium resulted in lung hypoplasia characterized by defective branching morphogenesis, altered cellular energetics and impaired epithelial maturation, culminating in neonatal lethality at birth from severe respiratory distress. Histological and biochemical analyses revealed expanded glycogen pools in the pulmonary epithelial cells at E18.5, concomitant with decreased pulmonary surfactant, suggesting a delay or an arrest in maturation. Importantly, these defects occurred in the absence of apoptosis or necrosis. In addition, sub-pleural hemorrhaging was evident as early as E14.5 in HIF1a TPM lungs, despite normal patterning of the blood vasculature, consistent with defects in endothelial barrier function. Epithelial expression of HIF1a TPM also resulted in increased VEGFA and VEGFC production, an increase in the number of lymphatic vessels and indirect activation of the multiple Notch pathway components in endothelial precursor cells. Collectively, these data indicate that HIF-1a protein levels in the pulmonary epithelium must be tightly controlled for proper development of the epithelial and mesenchymal compartments.

Keywords

lung; development; hypoxia; lymphangiogenesis; Notch; maturation

Introduction

Formation of the mammalian embryonic lung depends on many interdependent processes including branching of the endodermally-derived epithelium into the surrounding mesenchyme, development of the blood and lymphatic vasculature, and specification and maturation of multiple cell types within both tissue compartments. Previous studies have

[2]Corresponding Author: James P. Bridges, Division of Pulmonary Biology, Cincinnati Children's Hospital Medical Center, 3333 Burnet Avenue, ML7029, Cincinnati, OH 45229, Phone: (513) 636-0337, Fax: (513) 636-7868, James.Bridges@ccmhc.org.

demonstrated that the fetal lung is relatively hypoxic *in utero* (Lee et al., 2001), suggesting that low oxygen levels may promote lung organogenesis. Consistent with this concept, both branching morphogenesis and vascular development are enhanced in rodent lung explants exposed to a hypoxic environment relative to those cultured in ambient O_2 tensions (Gebb and Jones, 2003; Gebb et al., 2005; van Tuyl et al., 2005).

Organismal adaptation to low oxygen levels is primarily regulated at the transcriptional level by hypoxia-inducible factors (HIFs). HIFs are heterodimeric transcription factors comprised of an oxygen-sensitive alpha subunit (1a, 2a or 3a) and a constitutively expressed beta subunit (1b, also referred to as aryl hydrocarbon receptor nuclear translocator (ARNT)). All three alpha subunits, as well as ARNT, are critical modulators of embryonic mouse development as demonstrated in gene ablation studies (Maltepe et al., 1997; Iyer et al., 1998; Ryan et al., 1998; Compernolle et al., 2002; Scortegagna et al., 2003; Yamashita et al., 2008). HIF1a activity is largely regulated at the level of protein stability, governed by a family of prolyl hydroxylase domain (PHD)-containing enzymes, PHD1, 2 and 3 (Bruick and McKnight, 2001; Epstein et al., 2001; Ivan et al., 2002). Under normoxic conditions, the PHDs hydroxylate two conserved proline residues within the oxygen-dependent degradation domain (ODD) of human HIF1a, P402 and P564, in a process that requires O_2, Fe^{2+} and 2-oxoglutarate. Hydroxylated HIF1a is then recognized by the E3 ubiquitin complex von-Hippel-Lindau (pVHL), tagged with polyubiquitin and degraded by the 26S proteasome (see (Schofield and Ratcliffe, 2004) for review). In hypoxia, PHD-mediated hydroxylation is inhibited and HIF1a escapes proteasomal degradation. Stable HIF1a subunits then accumulate in the cytoplasm and translocate into the nucleus where they interact with ARNT. Functional HIF1a/ARNT dimers bind a conserved DNA binding motif known as the hypoxia responsive element (HRE) and activate a large number of target genes that regulate oxygen delivery, energy maintenance and survival (Wenger et al., 2005). In addition to regulation at the protein stability level, HIF1a transcriptional activity is also controlled via hydroxylation by the asparaginyl hydroxylase factor inhibiting HIF (FIH) (Mahon et al., 2001). Hydroxylation of HIF1a occurs at asparagine 803 (N803) and prevents interaction with the potent co-activator p300/CBP, thereby dampening the transcriptional activation of HIF1a under normoxic conditions (Ema et al., 1999; Lando et al., 2002b).

HIF1a protein is present at low levels in normoxia-cultured primary and transformed pulmonary cell types derived from multiple species and is highly induced under hypoxic conditions (Yu et al., 1998). Endogenous HIF1a and ARNT are primarily restricted to epithelial cells of the first trimester human fetal lung (Groenman et al., 2007), suggesting a role for epithelial HIF1a signaling in pulmonary development and/or maturation. In agreement, Cre-mediated deletion of HIF1a from the developing pulmonary epithelium using the *Sftpc*-rtTA/tetO7-Cre system has been reported to result in neonatal respiratory distress associated with decreased maturation of distal epithelial cells (Saini et al., 2008). In extremely premature infants, respiratory distress is a common morbidity resulting from insufficient maturation of the lung. This perturbation of maturation, coupled with mechanical ventilatory support, is thought to underlie the susceptibility of this patient population to developing a form of chronic lung disease known as bronchopulmonary dysplasia (BPD) (Baraldi and Filippone, 2007). Studies performed in large animal models of BPD have shown that HIF1a protein is decreased in the premature lung, associated with decreased vascularization and diminished levels of a pivotal HIF1a target gene, *Vegfa* (Asikainen et al., 2005; Asikainen et al., 2006b; Grover et al., 2007); chemical stabilization of HIF1a in the premature baboon model dramatically improved the pathophysiological pulmonary abnormalities (Asikainen et al., 2006a). Collectively, these data demonstrate that HIF1a signaling is required for the proper maturation and function of alveolar type II cells during fetal lung development.

The goals of the present study were to define the expression levels and localization patterns of endogenous HIF subunits during mouse lung development, to further define the functional role of HIF1a in the developing respiratory epithelium and to identify HIF1a target genes that mediate epithelial maturation. Toward these goals we generated transgenic mice that individually expressed two distinct normoxia-stable isoforms of HIF1a in the pulmonary epithelium in a conditional manner. Our results show that augmented expression of HIF1a in the developing pulmonary epithelium disrupts branching morphogenesis, associated with decreased epithelial cell proliferation, metabolic switching to a glycolytic phenotype and impaired maturation. HIF1a induction in the fetal respiratory epithelium also caused pulmonary vascular abnormalities, including hemorrhaging and a marked increase in lymphangiogenesis. These data demonstrate that excessive HIF1a activation in the fetal pulmonary epithelium resulted in developmental and maturational defects, suggesting that conditions that promote epithelial HIF1a stability and activation *in utero* may negatively impact pulmonary development and function.

Materials and Methods

Expression constructs and transgenic animals

The HIF1a ΔODD,N803A (amino acids 401–603 deleted, Asn803 mutated to Ala) and TPM constructs (Pro402, Pro564, and Asn803 mutated to Ala) were generated by PCR mutagenesis using human HIF1a cDNA as a template. A single HA-tag was cloned in frame to the C-terminus of both constructs by PCR. HA-tagged HIF1a ΔODD,N803A and TPM cDNAs were cloned into pcDNA3.1+ (Invitrogen, Carlsbad, CA) for use in transient transfection assays.

The HIF1a ΔODD,N803A transgenic construct was generated by subcloning the HIF1a ΔODD,N803A cDNA into the tetracycline-responsive pTRE-tight vector (Clontech, Mountain View, CA). The HIF1a TPM transgenic construct was generated in the following manner. First, the IRES sequence was PCR amplified from the pIRES2-EGFP vector (Clontech, Mountain View, CA) and cloned into the multiple cloning site of the $(teto)_7$CMV-bGH-poly(A) vector, kindly provided by Dr. Herman Bujard (Gossen and Bujard, 1992). Next, a FLAG-tagged human ARNT cDNA was cloned 3′ of the IRES sequence and the HIF1a TPM cDNA was cloned 5′ of the IRES sequence to generate the final construct. The constructs were linearized and microinjected individually into the pronucleus of fertilized eggs from FVB/N mice. The HIF1a ΔODD,N803A transgene was identified by PCR using the primers: 5′-AGCACGACTTGATTTTCTCCC-3′ and 5′-CATCCATTGATTGCCCCAG-3′. The HIF1a TPM transgene was identified using the primers: 5′-TGGATTACCACAGCTGACCA-3′ and 5′-AGGAACTGCTTCCTTCACGA-3′. To target the respiratory epithelium, the 3.7-kb human *Sftpc* promoter was used to drive the reverse tetracycline transactivator (*rtTA*). *hSftpc-rtTA* mice (line 1) (Perl et al., 2009) were mated to $(tetO)_7$*CMVHIF1a ΔODD,N803A* and $(tetO)_7$*CMVHIF1a TPM* mice to generate double transgenic *hSftpc-rtTA*$^{tg/wt}$, $(tetO)_7$*CMVHIF1a ΔODD,N803A*$^{tg/wt}$ (hereafter, HIF1a ΔODD,N803A) and *hSftpc-rtTA*$^{tg/wt}$, $(tetO)_7$*CMVHIF1a TPM*$^{tg/wt}$ (hereafter, HIF1a TPM) mice, respectively. The *hSftpc-rtTA* transgene was identified using the primers: 5′-GACACATATAAGACCCTGGTCA-3′ and 5′-AAAATCTTGCCAGCTTTCCCC-3′. The HIF1 transgenes were induced in respiratory epithelial cells of double transgenic mice by administering doxycycline in the food at a concentration of 525mg/kg dry weight (Harlan Teklad, Madision, WI) at times indicated in the Results section. Mice were maintained in a pathogen-free environment in accordance with protocols approved by the Institutional Animal Care and Use Committee of the Children's Hospital Research Foundation.

Generation of HIF1a antisera

The cDNA encoding amino acids 644–803 of human HIF1a protein was amplified from HIF1a WT/pcDNA3.1+ and cloned into the pET41a+ vector (Novagen) to create hHIF1a(644–803)/pET41a+. BL21(DE3) bacteria were transformed with hHIF1a(644–803)/pET41a+, grown to log phase and induced with 1mM IPTG for 4 hours to produce the recombinant protein. The protein was then isolated from lysed cells by nickel column purification and injected into guinea pigs with adjuvant to generate polyclonal antibodies. Primary sera were collected and passed through a GST column to adsorb anti-GST antibodies prior to use.

Saturated phosphatidylcholine (SatPC) and total glycogen assays

Embryonic lungs were placed in 0.9% saline and pulse sonicated on ice. Lipids were extracted from the samples by the Bligh and Dyer method (Bligh and Dyer, 1959). SatPC was isolated using the method of Mason et. al. (Mason et al., 1976) and quantitated by phosphorous measurement. Data were normalized to genomic DNA using a previously described method (Cesarone et al., 1979).

Total lung glycogen was measured using a modified method of Hassid and Abraham (Hassid and Abraham, 1957). Briefly, embryonic lung tissue was pulse sonicated on ice and boiled for 10min in anthrone reagent (0.2% anthrone (cat#AN135, Spectrum Chemical, Gardena, CA) in 95% sulfuric acid). The samples were then cooled on ice for 10 minutes and absorbance was measured at 620nM. Dilutions of D-glucose, ranging from 0.5μg – 200μg, were used to generate the standard curve. Data were normalized to genomic DNA content using an aliquot of the sample obtained prior to the glycogen assay.

Real-time PCR analysis

Whole-lung total RNA was purified by RNeasy Mini Kit (Qiagen, Valencia, CA) and reverse transcribed into cDNA with the iScript kit (BioRad, Hercules, CA). Quantitative RT-PCR (qPCR) was performed on a 7300 real-time PCR system (Applied Biosystems, Foster City, CA) with TaqMan probes (listed in Supplemental Data, Table I) and normalized to endogenous *ActB* for control (probe part number 4352933E). qPCR was performed with an *n* of 3–6 mice for each genotype.

Histology and immunohistochemistry (IHC)

Tissues were fixed in 4% paraformaldehyde, embedded in paraffin and 5μm sections were cut for H&E staining or IHC. Sections were processed with antigen retrieval using heating in citrate buffer. Primary antibodies used were: guinea pig anti-HIF1a (1:1000, generated in this laboratory); mouse anti-ARNT (1:200, cat#611078, BD Biosciences, Franklin Lakes, NJ); rabbit anti-Prox1 (1:200, cat#20R-PRO39, Fitzgerald Industries, Acton, MA); mouse anti-HA (1:100, cat#2367S, Cell Signaling, Danvers, MA); rabbit anti-mature SFTPB, rabbit anti-pro SFTPC and rabbit anti-ABCA3 (1:500–1:2000, Seven Hills Bioreagents, Cincinnati, OH); rat anti-CD34 (1:50, cat#ab8158, Abcam, Cambridge, MA); rabbit anti-phospho histone H3 (pHH3) (1:500, cat#sc8656r, SCBT, Santa Cruz, CA); rabbit anti-cleaved Notch1 (Val1744) (1:100, cat#2421, Cell Signaling, Danvers, MA); goat anti-Flt4 (1:100, cat#AF743, R&D Systems, Minneapolis, MN); mouse anti-Cdkn1a (1:250, cat#556430, BD Pharmingen, San Diego, CA). Biotinylated secondary antibodies were used with the ABC Vectastain kit (Vector Laboratories) for immunohistochemistry, fluorescent secondary antibodies were used for immunofluorescence. DAB with nickel enhancement was used for mature SFTPB, pro SFTPC, ABCA3, Prox1, Cdkn1a and HA staining followed by a nuclear fast red counterstain; DAB was used for HIF1, ARNT, pHH3 and CD34 with a hematoxylin counterstain.

Mitochondrial DNA assay

Total DNA was extracted from embryonic lung tissue. The amount of mitochondrial DNA relative to nuclear DNA was determined by qPCR analysis as described by Zhang et. al. (Zhang et al., 2008) using the following primers: *Nd2* (NADH dehydrogenase subunit 2, mitochondrial genome): FWD – CCCATTCCACTTCTGATTACC, REV – ATGATAGTAGAGTTGAGTAGCG; *Nme1* (non-metastatic cells 1, nuclear genome): FWD – CCTTCTTTACTGGCCTGGTG, REV – CGCACAGCTCTTGTACTCCA. Relative *ND2* copy number was calculated by the Livak method, using *Nme1* for normalization.

pHH3 morphometry

Cell counts of pHH3-positive cells were obtained by immunohistochemistry. Quantification was performed on lung sections from CON and HIF1a TPM mice (n=4 per group). Approximately 10–12 random high power fields were imaged from each animal (4 images per lobe) with the x- and y-coordinates of the images selected by a random number generator. The total number of pHH3-positive cells in the epithelium and the mesenchyme were counted manually and the raw data for each group were pooled.

Immunoblot analysis

Nuclear extracts were isolated from transfected HeLa cells using the NE-PER Nuclear Protein Extraction kit (Fisher Scientific, Pittsburgh, PA). Protein content was measured using a BCA protein assay (Fisher Scientific, Pittsburgh, PA). Nuclear extracts (50μg) were separated on 8% PAGEGels (Fisher Scientific, Pittsburgh, PA) for HIF1a and HA under reducing conditions. Blots were stripped and reprobed with anti-TFIIB (1:100, cat#sc-274, SCBT, Santa Cruz, CA) for loading control. Primary antisera included guinea pig anti-HIF1a (1:1000, generated in this laboratory), mouse anti-HA (1:1000, cat#2367S, Cell Signaling, Danvers, MA).

Transmission electron microscopy

The upper right lobes of E18.5 mouse lungs were fixed, processed and analyzed as previously described (Bridges et al., 2010).

Plasmid and luciferase reporter assays

The HRE-luc reporter plasmid was kindly provided by Roland Wegner (Gassmann et al., 1997). The VEGFp-luc reporter plasmid was kindly provided by Debabrata Mukhopadhyay (Mukhopadhyay et al., 1995). Luciferase assays was performed by transfecting HeLa cells with the HRE-luc/pGL3 or VEGFp-luc plasmid (200ng) along with empty vector control plasmid (pcDNA3.1+), HIF1a WT/pcDNA3.1+, HIF1a ΔODD,N803A/pcDNA3.1+ or HIF1a TPM/pcDNA3.1+ (50–250ng) using the transfection reagent Lipofectamine 2000 (Invitrogen, Carlsbad, CA). CMV-βGal plasmid was cotransfected to serve as an internal control, and luciferase activity was normalized to β-galactosidase activity after 24 hrs of transfection.

Isolation and culture of fetal lung mesenchyme

Distal lung mesenchyme was isolated from wild-type FVB/N mice at E12.5 as previously described (Hyatt et al., 2002). Briefly, distal lung tips were removed with Moria knives, treated with Dispase for 20 minutes at 37°C, rinsed 2X in ice-cold Hanks Buffered Salts + 10% FBS and treated briefly with DNase I. The epithelium was separated from the mesenchyme with fine tungsten needles. 5–7 pieces of mesenchyme were enrobed in 100μl drops of Cultrex® basement membrane extract (Trevigen, Gaithersburg, MD) and cultured in 10% DMEM/F12 supplemented with 100ng/ml recombinant FGF-9 (Peprotech, Rocky

Hill, NJ). Recombinant human VEGFA-165 and VEGFC(Cys156Ser) (R&D Systems, Minneapolis, MN) were added to the cultures at 20ng/ml as indicated. The gamma-secretase inhibitor DAPT (Sigma, St. Louis, MO) was added at 5μM as indicated.

Isolation and culture of adult type II cells

Mouse alveolar type II cells were isolated from 8-week old HIF1a TPM and CON mice (n=4 per genotype) and cultured on 100% Cultrex basement membrane extract as previously described (Rice et al., 2002). Cells were cultured for 3 days in BEGM containing 10% FBS and 10ng/ml KGF (Peprotech, Rocky Hill, NJ). On the forth day, doxycycline (1ug/ml) was added to the culture medium for 24hrs. The cells were harvested with dispase and processed for qPCR analysis as described.

VEGFA protein measurements

Individual E14.5 lungs were placed in PBS and pulse sonicated on ice. Total VEGFA protein was determined by ELISA (R&D Systems, Minneapolis, MN) and standardized to total protein content as determined by BCA assay.

Statistical analysis—All data are presented as means ± SEM with $p \leq 0.05$ considered significant. Multiple group comparisons were made by one-way ANOVA with a Tukey post-hoc analysis. Two-way comparisons were performed by two-tailed, unpaired Student's t-test. All analyses were performed using GraphPad Prizm software version 5.0.

Results

Ontogeny of HIF1a, EPAS1, NEPAS and ARNT in the developing mouse lung

To define the expression levels and localization patterns of hypoxia inducible factor subunits during mouse lung development, mRNA expression profiles in whole lung homogenates were analyzed by qPCR analysis. *HIF1a* mRNA levels were highest at E11.5 and generally decreased throughout development (Figure 1A). In contrast, *Epas1* levels were low from E11.5 through E17.5, increased significantly at PN1, with peak expression observed in adulthood (Figure 1B). *Nepas* mRNA levels were low at E11.5, peaked at E18.5 and were virtually undetectable by PN7 (Figure 1C), consistent with previous data (Yamashita et al., 2008). In contrast to the dynamic expression patterns of the HIF alpha subunits, *Arnt* mRNA levels were rather steady throughout prenatal lung development, followed by a 50% decrease at E17.5 through adulthood (Figure 1D).

We next defined the localization of HIF1a and ARNT protein in the developing lung by immunohistochemistry. As shown in Figure 1E, HIF1a protein was undetectable in the embryonic lung until E14.5, a stage at which weak nuclear staining was observed in the developing epithelium (white dotted circles). HIF1a protein levels were increased in the epithelium at E16.5 and E18.5. HIF1a protein was not detected in the mesenchyme at any stage of lung development. In contrast to HIF1a, ARNT protein was readily detected in both mesenchymal and epithelial cells at E12.5 and staining intensity steadily increased throughout gestation. Interestingly, ARNT expression was primarily restricted to the epithelial cells at E18.5.

Epithelial expression of HIF1a ΔODD,N803A during lung development results in perinatal lethality

To further define the role of HIF1a signaling during lung development, we generated transgenic mice that conditionally expressed a normoxia stable form of HIF1a in the pulmonary epithelium (*TRE*-HIF1a ΔODD,N803A) (Figure 2A). The HIF1a ΔODD,N803A

construct was engineered by deleting the oxygen-dependent degradation domain (ODD, amino acids 401–603) from the human HIF1a cDNA in order to prevent hydroxylation by the prolylhydroxylase PHD2, thereby circumventing proteasomal degradation of the ΔODD protein and promoting stabilization in normoxia as previously described (Huang et al., 1998; Elson et al., 2001). In addition, the conserved asparagine at position 803 was mutated to alanine to prevent hydroxylation by factor inhibiting HIF (FIH), leading to enhanced transcriptional activity of the protein in normoxic conditions (Lando et al., 2002a; Lando et al., 2002b). The completed ΔODD,N803A transgene was then placed under control of the tetracycline-responsive element (TRE) and transgenic animals (hereafter *TRE*-HIF1a ΔODD,N803A mice) were generated using standard methodologies.

To determine the effects of expressing a stabilized form of HIF1a in the developing pulmonary epithelium, *TRE*-HIF1a ΔODD,N803A mice were mated with *Sftpc*-rtTA activator mice and placed on doxycycline from E6.5 to birth. A total of 67 newborn pups were obtained from these crosses, 25 of which were double transgenic for the *Sftpc*-rtTA and *TRE*-HIF1a ΔODD,N803A transgenes (37%). Of these 25 animals, 21 (84%) were either found dead at birth or succumbed shortly thereafter, exhibiting classical signs of respiratory distress including cyanosis and labored breathing. Histological analyses of lung tissue from mice that died shortly after birth revealed the presence of proteinaceous material in the airspaces and decreased mesenchymal thinning, pathological abnormalities that are also consistent with severe respiratory distress and atelectasis (Figure 2B). Analysis of lung tissue at E18.5, one day prior to birth, demonstrated no aberrant histological abnormalities in ΔODD,N803A mice compared to controls.

To determine if the observed phenotype could be attributed to decreased or arrested maturation of the distal epithelium, multiple markers of distal epithelial cell maturation were analyzed. Immunohistochemical analyses demonstrated widespread expression of the ΔODD,N803A transgene in pulmonary epithelial cells, as determined by HA staining (Figure 2C). Expression of mature surfactant protein B (SFTPB), pro-surfactant protein C (SFTPC) and the phospholipid transporter ATP-binding cassette subfamily A member 3 (ABCA3) were all decreased in ΔODD,N803A animals compared to controls (Figure 2C). Furthermore, total saturated phosphatidylcholine (SatPC), the primary surface active component of pulmonary surfactant, was decreased 21% compared to littermate controls (Figure 2D). qPCR analyses demonstrated that several known HIF1a target genes were induced in ΔODD,N803A lungs at E14.5 including the glucose transporters *Slc2a1* and *Slc2a3*, and the glycolytic enzymes *Pgk1*, *Car9*, and *Hk2* (Figure 2E). Two additional HIF1 targets, *Serpine1* and *Vegfa*, were not significantly induced by epithelial ΔODD,N803A expression. Taken together, these data demonstrate that epithelial expression of the HIF1a ΔODD,N803A protein in the developing lung results in severe respiratory distress in a majority of the animals at birth. This pathophysiological phenotype is associated with the transcriptional activation of a glycolytic program and arrested epithelial maturation, as evidenced by decreased expression of several distal epithelial markers, including mature SFTPB, pro SFTPC and ABCA3, and decreased levels of SatPC.

HIF1a triple point mutant (TPM) stability and transactivation potential compared to ΔODD,N803A

While the ΔODD,N803A protein is more stable and transcriptionally active in normoxia compared to the wild type protein, we hypothesized that deletion of the 202 amino acid ODD domain from HIF1a may result in a misfolded protein that could negatively impact cell function. Therefore, as an alternative approach to the ΔODD,N803A construct, we generated a second stable HIF1a isoform by specifically mutating the proline residues that confer degradation of HIF1a in normoxia, P402 and P564, and asparagine 803 to alanine. This resultant construct is referred to as HIF1a triple point mutant (TPM) (Figure 4A) and is

identical to the previously reported P1P2N HIF1a and HIF1a PPN constructs (Dioum et al., 2008; Bekeredjian et al., 2010). To distinguish the transfected proteins from endogenous HIF1a, all three constructs (wild type (WT), ΔODD,N803A and TPM) contained an in-frame, C-terminal HA tag.

The relative stability and transactivation potential of the two stabilized isoforms, HIF1a ΔODD,N803A and HIF1a TPM, were compared to HIF1a WT by immunoblot analysis of nuclear extracts from transiently transfected HeLa cells cultured under normoxic and hypoxic ($1\%O_2$) conditions for 17 hours (Figure 3). As shown in Figure 3A, HIF1a TPM is more stable in normoxia than the WT and ΔODD,N803A isoforms (compare lane 7 vs. lanes 3 and 5, HIF1a blots). In addition, the TPM protein is hypoxia-insensitive (lanes 7 vs. 8, HA blot), similar to the ΔODD,N803A isoform (lanes 5 vs. 6, ΔODD,N803A band in HIF1a blots). Surprisingly, expression of the ΔODD,N803A isoform inhibited the hypoxic induction of endogenous HIF1a in HeLa cells (compare lanes 5 and 6 to lanes 1 and 2, HIF1a band in HIF1a blots).

Transient transactivation assays using two HIF responsive promoter constructs, hypoxia responsive element (HRE) HRE-luciferase and the proximal promoter of the human VEGF gene (VEGFp) VEGFp-luciferase, demonstrated that the activity of the TPM isoform was 7-fold higher than WT and 4-fold higher than ΔODD,N803A (Figure 3B). In addition, co-transfection of ARNT with the HIF1a constructs potentiated the transactivation response of all isoforms ~3 fold on the HRE-luciferase and VEGFp-luciferase promoters, demonstrating that ARNT availability may be limiting, depending on the cell type (Figure 3C).

Epithelial expression of HIF1a TPM during lung development perturbs lung morphogenesis and distal epithelial cell maturation

Based on the in vitro expression data demonstrating increased stability and transactivation potential of the HIF1a TPM, we generated conditional HIF1a TPM transgenic mice (*TRE*-HIF1a TPM) (Figure 4A). Since the pulmonary epithelium expresses HIF1a, EPAS1 and NEPAS, all of which dimerize with ARNT, the HIF1a TPM construct was also engineered to contain an IRES sequence that allowed expression of a FLAG-tagged ARNT cDNA downstream of HIF1a TPM. Using this strategy, HIF1a TPM and ARNT protein are generated in a 1:1 ratio from a single mRNA transcript, thereby preventing HIF1a TPM from acting as a sink for endogenous ARNT protein, avoiding a possible dominant negative effect on endogenous HIF1a, EPAS1 and/or NEPAS function.

HIF1a TPM protein was expressed in the embryonic pulmonary epithelium by mating *TRE*-HIF1a TPM mice to *Sftpc*-rtTA mice and placing the pregnant dams on doxycycline chow from E6.5 until harvest at E18.5. As shown in Figure 4B, expression of HIF1a TPM disrupted branching morphogenesis, resulting in large dilated cysts in the peripheral lung at E18.5. Single transgenic (*Sftpc*-rtTA or *TRE*-HIF1a TPM) or wild-type littermates did not exhibit any morphological abnormalities and were used interchangeably as controls (CON). Histological analysis demonstrated the presence of hypertrophic cells in the distal epithelium and eosin-positive proteinaceous material filling the primitive air sacs in HIF1a TPM lungs, indicative of vascular leak (Figure 4C, H&E). Interestingly, only a small percentage of epithelial cells stained positively for HA and HIF1a protein in the HIF1a TPM lungs at this stage, suggesting that the transgene was either extinguished by the time of analysis, or that transgene-positive cells underwent apoptosis or necrosis. Staining for cleaved caspase 3 was negative in HIF1a TPM lungs at this stage and nuclear morphology of the epithelium was normal as assessed by Hoechst staining, indicating that the low number of HIF1a TPM-positive cells was not due to apoptosis or necrosis (data not shown). To determine if epithelial maturation was altered, pro SFTPC immunohistochemistry was performed. The results indicated that pro SFTPC protein expression was drastically reduced in the HIF1a

TPM epithelium compared to controls, suggesting impaired expansion or maturation of this lineage (Figure 4C, pro SFTPC). Consistent with these findings, qPCR analysis demonstrated a 25–50% decrease in four markers of distal epithelial cell maturation including *Pdpn, Lpcat1, Sftpb and Sftpc* (Figure 4D). Since the HIF1a TPM transgene was driven from the *Sftpc* promoter in this experiment, the most likely explanation for the low number of transgene-positive cells was decreased SFTPC expression.

To further characterize the maturational state of the pulmonary epithelium in HIF1a TPM mice, lungs were processed for electron microscopy. Toluidine blue-stained, semi-thin sections and electron micrographs showed abundant secreted surfactant in the airspaces of CON lungs at E18.5 (Figure 5A and 5C, arrows). In addition, alveolar type II cells of CON animals contained numerous mature lamellar bodies and minimal glycogen stores (Figure 5C, arrowheads). In contrast, the airspaces of HIF1a TPM mice were devoid of secreted surfactant (Figure 5B) and mature lamellar bodies were absent in the distal epithelial cells. Instead, abundant glycogen stores were readily observed in HIF1a TPM epithelial cells, consistent with impaired maturation. Glycogen assays on E18.5 lungs demonstrated a 2.1-fold increase in total lung glycogen in HIF1a TPM lungs (Figure 5E). Since glycogen serves as the substrate for surfactant phospholipid biosynthesis, it was not surprising that the lack of depletion of glycogen was accompanied by a concomitant 2.3-fold decrease in tissue SatPC levels (Figure 5F). Collectively, these data indicate that continuous HIF1a TPM expression in the developing epithelium impairs distal epithelial cell maturation, resulting in severe dysmorphogenesis at E18.5.

Defective branching morphogenesis, hemorrhaging and induction of a glycolytic switch in HIF1a TPM lungs at E14.5

To determine the time point at which epithelial HIF1a TPM expression first induces lung dysmorphogenesis, the HIF1a TPM transgene was activated *in utero* from E6.5 until harvest at E12.5 or E14.5. Branching morphogenesis was unaltered in lungs that expressed HIF1a TPM from E6.5 to E12.5 (n=6–8 per genotype, data not shown). In contrast, severe defects were noted in the HIF1a TPM lungs at E14.5 including overall hypoplasia, decreased branching of the developing airways and prominent subpleural hemorrhaging (Figure 6A). In contrast to the mosaic expression pattern of the transgene at E18.5 (Figure 4B), HIF1a TPM protein was readily detected in a majority of epithelial cells at E14.5, as seen by anti-HA and anti-HIF1a immunohistochemistry (Figure 6B). Increased ARNT protein was also detected in the epithelial cells of HIF1a TPM mice, indicating expression of the ARNT transgene (Figure 6B, ARNT staining, arrowheads).

HIF1a expression has been shown to inhibit energy-expensive processes such as cell proliferation, thereby preserving adequate ATP levels to ensure cell survival (Chandel, 2010). To determine if HIF1a expression inhibited epithelial cell proliferation in HIF1a TPM mice, phospho-histone H3 (pHH3) staining was performed on E14.5 lung sections. As shown in Figure 7A and 7B, pHH3 staining was significantly decreased in the epithelium of HIF1a TPM lungs but not in the mesenchymal cell compartment. HIF1a has been shown to inhibit cell cycle progression via increased expression of Cdkn1a (Koshiji et al., 2004). Therefore, we examined the expression of the cell cycle inhibitors Cdkn1a and Cdkn1b in HIF1a TPM lungs at E14.5. Cdkn1a mRNA was increased 2.9-fold in HIF1a TPM lungs while Cdkn1b levels remain unchanged (Figure 7C). In accordance, Cdkn1a protein was highly induced in the epithelium of HIF1a TPM mice (Figure 7D). Both Cdkn1a and Cdkn1b levels were unchanged in HIF1a ΔODD,N803A at E14.5 (Supplemental Figure 2). These data suggest that the hypoplastic and impaired branching phenotype is due, in part, to an inhibition of cell cycle progression in the developing epithelium of HIF1a TPM mice.

H&E staining of E14.5 lungs revealed the presence of hypertrophic epithelial cells that stained negatively for eosin (Figure 8A), similar to what was observed when the transgene was expressed from E6.5 to E18.5 (Figure 4C). Accordingly, total lung glycogen content was found to be increased 2.5-fold in HIF1a TPM lungs (Figure 8B). The increased glycogen content at this stage of development suggested that HIF1a TPM expression in the developing epithelial cells induced a metabolic shift toward a glycolytic phenotype, a known HIF1a-dependent event (Iyer et al., 1998). To test this hypothesis, glycolytic enzymes that are known HIF1a targets were measured in HIF1a TPM lungs by qPCR analysis. HIF1a TPM induced the expression of several glycolytic genes including *Aldoc*, *Slc2a1*, *Slc2a3*, *Pdk1* and *Pgk1* (Figure 8C). Interestingly, expression of *Bhlhe40*, a transcription factor with known anti-apoptotic and anti-lipogenic properties (Li et al., 2002; Yun et al., 2002), was induced 3.5-fold in HIF1a TPM lungs.

Given the known role of HIF1a in regulating mitochondrial homeostasis (Zhang et al., 2007; Zhang et al., 2008), the total mitochondrial content of HIF1a TPM lungs was measured and compared to CON lungs. Surprisingly, the mitochondrial content of HIF1a TPM lungs was decreased 3.2-fold compared to CON lungs (Figure 8D). In addition, the mRNA levels of the cytochrome oxidase C subunit 4i2 gene (*Cox4i2*), a known HIF1a target that optimizes flux through the electron transport chain and minimizes the generation of reactive oxygen species under hypoxic conditions (Fukuda et al., 2007), were also increased 3.0-fold in HIF1a TPM lungs (Figure 8E). Taken together, these data demonstrate that HIF1a TPM expression in the pulmonary epithelium induced a metabolic shift toward a glycolytic phenotype, as evidenced by induction of several glycolytic enzymes, a net increase in glycogen content, decreased mitochondrial content and Cox4 subunit switching.

Compromised vascular integrity in HIF1a TPM embryonic lungs

The basis for the subpleural hemorrhaging observed in E14.5 HIF1a TPM lungs (Figure 6A) was explored in further histological detail. The blood pooling was primarily subpleural in nature, localized to the area immediately subtending the lung mesothelium (Figure 9A, arrowheads). To determine if vascular patterning was grossly disrupted by epithelial HIF1a TPM expression, the *Tek*-lacZ allele was crossed into the HIF1a TPM and CON mice. The *Tek*-lacZ transgene is a pan-endothelial marker expressed on arterial, venous and lymphatic endothelial cells, and therefore serves as a robust tool to visualize vascular development (Schlaeger et al., 1997). Whole mount β-galactosidase assays of *Tek*-lacZ/HIF1a TPM and *Tek*-lacZ/CON lungs indicated that global vascular patterning was normal in HIF1a TPM lungs at E14.5, including appropriate formation of the vascular plexus enrobing the developing epithelial buds (Figure 9A, *Tek*-lacZ). To further confirm normal patterning of the vasculature, CD34 immunohistochemistry was performed on paraffin-embedded sections. In concordance with the Tek-lacZ data, the association of CD34-positive endothelium with the surrounding epithelium was not grossly perturbed in HIF1a TPM lungs (Figure 9A, CD34 insets). While the overall density of CD34-positive staining appeared to be decreased in HIF1a TPM lungs, the degree of staining correlated with the decreased number of epithelial buds. These data suggested that the subpleural hemorrhaging was due to compromised endothelial barrier function as opposed to defects in patterning of the pulmonary vasculature.

Given that VEGFA is a direct transcriptional target of HIF1a and has known vessel permeability-promoting properties, we measured the levels of *Vegfa* isoforms in HIF1a TPM lungs by qPCR analysis. Significant increases in the $Vegfa_{164}$ and $Vegfa_{188}$ isoforms were observed, as was a modest increase in the lymphangiogenic promoting VEGF family member, *Vegfc* (Figure 9B). The increased *Vegfa* mRNA levels in the HIF1a TPM lungs correlated with a 2.2-fold increase of total VEGFA protein levels in whole lung homogenate (Figure 9C). To determine if HIF1a TPM-dependent increases in *Vegfa and Vegfc* were cell

autonomous, type II epithelial cells were isolated from adult HIF1a TPM and CON animals that had not been exposed to dox *in vivo* and cultured *in vitro*. Activation of HIF1a TPM in isolated type II epithelial cells induced Vegfa and Vegfc mRNA to levels that were higher than that seen in whole lung homogenates, demonstrating that HIF1a induces these genes in the epithelium (Figure 9D). Of note, VEGFA protein levels in lung homogenates of E14.5 HIF1a ΔODD,N803A mice did not differ from littermate controls, consistent with the lack of a hemorrhagic phenotype in this model (Supplementary Figure 1B). Collectively, HIF1a TPM expression increases VEGFA and VEGFC expression in type II cells of HIF1a TPM mice and while gross vascular patterning is unaffected in these animals, endothelial barrier function appears to be disrupted as evidenced by profound subpleural hemorrhaging.

Epithelial expression of HIF1a TPM induces lymphangiogenesis in the embryonic lung

Based on the observation that HIF1a TPM expression induced *Vegfc* transcription, we next determined if lymphangiogenesis was increased in HIF1a TPM lungs at E14.5. As an initial index, we quantified a panel of lymphangiogenic markers in HIF1a TPM lungs and found that the transcription factors *Prox1, Foxc2, Sox17* and *Sox18* were all increased in HIF1a TPM lungs, in addition to *Ccl21a*, a chemokine that is produced by lymphatic endothelial cells (Figure 10A) (Bromley et al., 2005). These findings were supported by Prox1 immunohistochemistry data, which demonstrated an increased number of Prox1-positive endothelial cells in HIF1a TPM pulmonary vessels compared to CON (Figure 10C vs. 10B, arrows in insets). Since Prox1 is also expressed in pulmonary neuroendocrine cells at this stage of development (Figure 10B and C, arrowheads in insets), dual immunofluorescence for Prox1 and FLT4 was performed to denote definitive lymphatic vessels. Note the dramatic increase in the number and size of dual-positive lymphatic vessels in the HIF1a TPM lungs compared to CON (Figure 10E vs. 10D, arrowheads).

Due to the known role of Notch signaling in blood vessel specification, we measured the expression of a number of Notch pathway components in HIF1a TPM lungs and found that two of the four Notch receptors, *Notch3* and *Notch4*, were modestly increased, as was the Notch ligand *Jag1*. In addition, three downstream Notch effectors, *Hey1, Hey2* and *Heyl*, were also increased (Figure 10F). We also measured the expression of Notch signaling components in HIF1a ΔODD,N803A mice at E14.5 (Supplementary Figure 1A). Both the repertoire and extent of induction differed between the HIF1a TPM and ΔODD,N803A lungs. Specifically, in HIF1a ΔODD,N803A lungs the receptors *Notch1* and *Notch4* were induced, as were the effectors *Hey1* and *Heyl*, while *Notch3*, *Jag1* and *Hey2* levels remained unchanged.

HIF1a is known to potentiate Notch1 signaling through direct protein-protein interactions with the Notch1 intercellular domain (NICD) (Gustafsson et al., 2005; Sahlgren et al., 2008). To discern whether HIF1a TPM expression was directly potentiating Notch1 signaling in the epithelium, immunofluorescent staining was performed with the Notch1 Val1744 antibody as a readout for active Notch1 signaling (Del Monte et al., 2007). As shown in Figure 10G, active Notch1 signaling was not detected in the epithelium of E14.5 control mice, consistent with previous data (Morimoto et al., 2010), and HIF1a TPM expression did not induce Notch1 signaling in the epithelium. However, HIF1a TPM expression did increase the basal Notch1 Val1744 staining seen in the mesenchyme immediately subtending the epithelium of CON lungs (Figure 10G, arrows), indicating that epithelial HIF1a expression indirectly activates Notch1 signaling in mesenchymal cells.

VEGFA and VEGFC are sufficient to induce Notch-dependent activation of lymphangiogenic markers in fetal lung mesenchyme

In order to determine if VEGFA and VEGFC were sufficient to induce lymphangiogenic markers in lung mesenchymal cells independent of lung epithelium, fetal lung mesenchyme was isolated from E12.5 mouse lungs and cultured on basement membrane extract in the presence of exogenous FGF9 to promote survival and expansion of this tissue in culture (del Moral et al., 2006; White et al., 2006) (Figure 11A). Recombinant human VEGFA-165 or the FLT4-specific VEGFC protein, VEGFC(Cys156Ser), was added to the mesenchyme cultures on d2 in the presence or absence of the Notch inhibitor DAPT. The mesenchyme was then harvested on d3 for qPCR analysis of lymphangiogenesis markers and Notch pathway components. As shown in Figure 11B, both exogenous VEGFA-165 and VEGFC(Cys156Ser) protein induced expression of the lymphangiogenic transcription factors *Foxc2* and *Sox18* while expression of *Prox1* was not affected. The Notch pathway downstream effector genes shown to be induced in HIF1a TPM lungs, *Hey1* and *Heyl*, were also induced by exogenous VEGFA or VEGFC-treated isolated mesenchyme. Interestingly, both VEGFA- and VEGFC-induced upregulation of *Foxc2, Sox18, Hey1* and *Heyl* were completely suppressed by co-treatment with the Notch pathway inhibitor, DAPT (Figure 11B). Collectively, these data are consistent with a model in which activation of epithelial HIF1a protein leads to increased expression and secretion of VEGFA and VEGFC from the pulmonary epithelium (Figure 11C). The secreted VEGFA and VEGFC ligands then engage their cognate receptors, KDR and FLT4 respectively, on neighboring endothelial precursor cells, leading to the downstream activation of Notch signaling on adjacent endothelial cells. This activation of Notch receptors then leads to the induction of a lymphangiogenic pathway, as evidenced by increased expression of Sox18, Foxc2, Hey1 and Heyl.

Discussion

Our goal in this study was to further define the role of HIF1a in the pulmonary epithelium during lung organogenesis. Our data demonstrate that endogenous expression of HIF1a protein is primarily restricted to epithelial cells in the developing murine lung, with expression first detected at E14.5; in contrast, expression of ARNT, the obligate transcriptional binding partner of HIF1a, was detected in both mesenchymal and epithelial cells at E12.5 and expression was maintained throughout lung development. Transgenic expression of a normoxia-stable and transcriptionally-enhanced isoform of HIF1a, HIF1a ΔODD,N803A, in the developing epithelium did not impair branching morphogenesis, but instead resulted in respiratory distress and significant lethality at birth. The impaired respiratory phenotype in HIF1a ΔODD,N803A mice was associated with reduced SatPC content and decreased expression of several genes that are critical for surfactant production and function, including *Sftpc, Sftpb and Abca3.* In contrast, transgenic expression of an alternative normoxia-stable, transcriptionally-enhanced HIF1a isoform, HIF1a TPM, in the epithelium drastically disrupted branching morphogenesis, associated with decreased epithelial proliferation, a metabolic shift toward a glycolytic phenotype and impaired epithelial maturation. Moreover, HIF1a TPM expression resulted in pulmonary vascular abnormalities, including subpleural hemorrhaging and a marked increase in lymphangiogenesis. These phenotypes were associated with increased VEGFA and VEGFC production and activation of Notch signaling pathways. Collectively, these data indicate that excessive HIF1a activation in the fetal pulmonary epithelium results in developmental and maturational defects, suggesting that conditions that promote epithelial HIF1a stability and activation *in utero* may negatively impact pulmonary development and function.

Previous work from our lab has shown that the threshold level of SatPC required for perinatal lung function in mice lies between 4.3 and 5.6nmol/mg tissue weight, amounts that represent 46.0–60.0% of wild-type levels (Bridges et al., 2010). Based on these data, it is

unlikely that the 21% decrease in SatPC levels seen in HIF1a ΔODD,N803A mice solely underlies the respiratory distress and neonatal lethal phenotype. However, this deficiency in SatPC production, combined with substantial decreases in mature SFTPB and ABCA3 protein expression, both of which are required for the transition to air breathing (Clark et al., 1995; Ban et al., 2007; Fitzgerald et al., 2007; Hammel et al., 2007), may have been sufficient to induce respiratory distress at birth. We do not believe that the HIF1a-mediated inhibition of SFTPB and ABCA3 expression is direct, since HIF1a TPM expression did not suppress baseline expression of the proximal *Sftpb* and *Abca3* promoters in luciferase reporter assays (data not shown). An alternative explanation for the observed phenotype is that the HIF1a ΔODD,N803A protein inhibited endogenous HIF1a function in the developing respiratory epithelium of HIF1a ΔODD,N803A transgenic mice. This possibility stems from our observation that transient HIF1a ΔODD,N803A expression in HeLa cells decreased the hypoxic induction of endogenous HIF1a protein (Figure 3A). In support of this hypothesis, genetic deletion of HIF1a in the developing respiratory epithelium resulted in phenotypic similarities seen in HIF1a ΔODD,N803A mice, including decreased production of surfactant proteins SFTPB and SFTPC and the phospholipid transporter ABCA3 in distal epithelial cells without defects in branching morphogenesis (Saini et al., 2008).

Epithelial HIF1a TPM expression profoundly affected branching morphogenesis, characterized by hypoplasia and the presence of a cystic distal epithelium that was initially detected at E14.5 and persisted throughout lung organogenesis. One possible explanation for this morphogenetic defect is decreased proliferation of HIF1a TPM-expressing epithelial cells (Figure 7A and 7B). During early embryonic lung development, the rate of cell proliferation is highest in the epithelial cells located at the branch points where it drives both growth and patterning of the developing airways (Hogan and Yingling, 1998; Warburton et al., 2000). *In vitro* studies have shown that prolonged hypoxic exposure induces HIF1a-dependent cell cycle arrest in a variety of cell types (Gardner et al., 2001; Green et al., 2001; Goda et al., 2003; Koshiji et al., 2004). Arrest occurs at the G1/S transition and is driven by increased expression of the cell cycle regulators *Cdkn1a*, via HIF1a-mediated displacement of the C-Myc repressor from the *Cdkn1a* promoter, and direct transcriptional activation of *Cdkn1b* (Gardner et al., 2001; Goda et al., 2003). In the HIF1a TPM transgenic mice, *Cdkn1a* was induced in the epithelium whereas *Cdkn1b* levels were unchanged (Figure 7C and 7D). Importantly, both *Cdkn1a* and *Cdkn1b* levels were not induced in HIF1a ΔODD,N803A mice (Supplementary Figure 2), in which branching proceeded normally, suggesting that the differential transcriptional induction of *Cdkn1a* in HIF1a TPM mice underlies the branching defect. In addition to the induction of *Cdkn1a*, it is likely that the decreased mitochondrial content and metabolic shunting toward glycolysis also contributed to decreased epithelial proliferation by limiting the amount of ATP required for this energy expensive process. Interestingly, genetic deletion of another Myc family member, N-Myc, resulted in a similar cystic phenotype that was associated with decreased epithelial cell proliferation (Moens et al., 1992; Moens et al., 1993; Sawai et al., 1993; Okubo et al., 2005). Whether the decreased proliferation observed in the HIF1a TPM respiratory epithelium is also due, in part, to an N-Myc-dependent mechanism remains to be determined.

The blood vascular defects in HIF1a TPM lungs did not appear to be due to hypervascularity or gross alterations in patterning of the vascular plexus. One possible explanation for the subpleural hemorrhaging is the HIF1a-mediated induction of endogenous VEGFA protein from the epithelial cells, resulting in increased permeability of the blood vasculature. This hypothesis is consistent with previous reports demonstrating an accumulation of interstitial fluid in transgenic mice that overexpressed the mouse $VEGFA_{164}$ isoform in developing (Zeng et al., 1998) or postnatal (Le Cras et al., 2004) pulmonary epithelial cells, and in adult lungs in which human VEGF-165 was ectopically expressed by adenoviral infection (Kaner

et al., 2000). In addition, HIF1a ΔODD,N803A mice, in which blood vascular integrity was normal, did not have elevated VEGFA levels (Supplemental Figure 1A). Gain of HIF1a function in the epidermis, using two distinct HIF1a transgenic constructs and epidermal promoters, increased endogenous VEGFA levels and was associated with a vascular phenotype that was distinct from our model, characterized by hypervascularity in the absence of baseline microvascular leak (Elson et al., 2001; Oladipupo et al., 2011). Many mechanistic differences could be responsible for the discrepancy between the HIF1a-mediated phenotype in the pulmonary and epidermal vascular tissue beds including: 1) potency of HIF1a transgenic constructs; 2) differential VEGF receptor expression on endothelial cells in the developing lung compared to the epidermis; 3) differences in VEGFA isoform expression between the models or 4) dysregulation of alternative pathways that modulate vascular permeability independent of VEGFA. Determining the mechanistic basis underlying the sensitivity of the pulmonary microvasculature to HIF1a-mediated permeability requires further investigation.

The increased lymphangiogenesis in the HIF1a TPM mice was a surprising observation. Previous data had shown that conditional induction of the $VEGFA_{164}$ isoform in the pulmonary epithelium during the pseudoglandular stage of development was sufficient to induce a 3-fold increase in lymphangiogenesis (Mallory et al., 2006). In our model, HIF1a TPM induced expression of $VEGFA_{164}$, but also increased expression of the $VEGFA_{188}$ isoform and another VEGF family member, VEGFC, a bona fide lymphangiogenic growth factor (Karkkainen et al., 2004; Lohela et al., 2008). Furthermore, we observed activation of Notch1 signaling in the lung mesenchyme and induction of several Notch pathway components that are known modulators of blood and lymphatic endothelial cell specification (Figure 10F&G, see (Rocha and Adams, 2009) for review). *Ex vivo* experiments using epithelium-free fetal lung mesenchyme demonstrated that recombinant VEGFA-165 and VEGFC were independently sufficient to induce the Notch effectors *Hey1* and *Heyl*, and the lymphatic markers *Foxc2* and *Sox18*, but not *Prox1* (Figure 11B). In addition, induction of these lymphatic markers by VEGFA or VEGFC was prevented by co-treatment of the mesenchyme with the Notch inhibitor DAPT. Collectively, these data suggest a model whereby HIF1a TPM-mediated lymphangiogenesis is mediated by increased VEGFA and/or VEGFC secretion by the epithelium, engaging the KDR and/or FLT4 receptors on endothelial precursor cells in the fetal lung mesenchyme. KDR and/or FLT4 engagement then activates Notch signaling in an adjacent endothelial precursor cell to govern it toward a lymphatic endothelial cell fate (Figure 11C).

Fetal lung development occurs in a relatively hypoxic environment (Gao and Raj, 2010), suggesting that low oxygen tension promotes organogenesis. Consistent with this concept, *ex vivo* studies performed with rodent lung explants demonstrate that both airway branching and vascular morphogenesis are increased when cultured in a hypoxic environment (Gebb and Jones, 2003; Gebb et al., 2005; van Tuyl et al., 2005). Using an oligodeoxynucleotide knockdown approach, Van Tuyl et. al. demonstrated that the hypoxia-mediated increase in branching and vascular morphogenesis observed in their model were mediated by HIF1a (van Tuyl et al., 2005). These data, in conjunction with the epithelial localization of HIF1a protein in the developing mouse and human lung (Figure 1E and (Groenman et al., 2007)), led us to hypothesize that the hypoxia-induced phenotype seen *ex vivo* was driven by increased expression of HIF1a in the epithelium. However, in our transgenic model, epithelial HIF1a TPM expression resulted in the opposite phenotype, characterized by decreased airway branching and vascular leak. Several possibilities exist for which to explain these phenotypic differences. First, the level of epithelial HIF1a expression in the HIF1a TPM mice may have been higher than that observed in hypoxia-cultured lungs, thereby activating alternative molecular pathways or amplifying overlapping pathways that result in distinct phenotypes. Second, although the expression pattern of HIF1a in hypoxia-

cultured lungs was not reported at the cellular level (van Tuyl et al., 2005), one would predict that all cells within the lung would stabilize HIF1a protein since HIF1a mRNA is ubiquitously expressed. Therefore, an alternative explanation is that hypoxia-induced HIF1a expression in the mesenchymal cells of the explant model promotes branching and hypervascularity. Third, it is also possible that HIF1a-independent hypoxia effects, including stabilization of EPAS1, activation of the unfolded protein response and downstream target genes (Koritzinsky et al., 2006) and/or increased translation of selective mRNAs including VEGFA (Young et al., 2008), contributed to the hypoxia-mediated increase in airway branching and vascular morphogenesis *ex vivo* that was not observed in our model. Lastly, although the HIF1a TPM protein is more stable and transcriptionally active that wild type HIF1a (Figure 3), its structure and/or function may differ from that of endogenous HIF1a, contributing to the observed phenotype.

It has been demonstrated that HIF1a protein and several HIF1a target genes, including *Vegfa*, *Vegfc* and *Bhlhb2*, are increased in patients with two distinct forms of chronic lung disease, idiopathic pulmonary fibrosis (IPF) and cryptogenic organizing pneumonia, and in a bleomycin-induced animal model of pulmonary fibrosis (Tzouvelekis et al., 2007). In the IPF lung, HIF1a protein is primarily localized to the alveolar epithelial cells immediately overlying or adjacent to the fibroblastic foci, the histological hallmarks of this disease. Increased lymphangiogenesis has also reported in patients with IPF and in the bleomycin-induced pulmonary fibrosis model (Teles-Grilo et al., 2005; El-Chemaly et al., 2009). While total VEGFA, VEGFC and VEGFD levels were not increased in bronchoalveolar lavage fluid from IPF patients, it may be the local bioavailability of these pro-lymphatic factors, or the VEGFR3 receptor itself, that is important in promoting the lymphangiogenic process. Although these observations are correlative in nature, it is tempting to speculate that stabilization of HIF1a protein in the early stages of the fibrotic process drives lymphangiogenesis in the IPF lung via the VEGF and Notch signaling pathways, potentially contributing to the pathophysiology of disease.

Supplementary Material

Refer to Web version on PubMed Central for supplementary material.

Acknowledgments

The authors would like to thank Xiaofei Shangguan, Mike Burhans, Kalpana Srivastava, Shawn Grant and Angelica Schehr for excellent technical assistance and/or advice.

This work is supported by NIH awards HL-084376 and HL-029891 to JMS. JPB is supported through a postdoctoral fellowship from the Parker B. Francis Foundation.

Bibliography

Asikainen TM, Ahmad A, Schneider BK, White CW. Effect of preterm birth on hypoxia-inducible factors and vascular endothelial growth factor in primate lungs. Pediatr Pulmonol. 2005; 40:538–546. [PubMed: 16231377]

Asikainen TM, Chang LY, Coalson JJ, Schneider BK, Waleh NS, Ikegami M, Shannon JM, Winter VT, Grubb P, Clyman RI, Yoder BA, Crapo JD, White CW. Improved lung growth and function through hypoxia-inducible factor in primate chronic lung disease of prematurity. FASEB J. 2006a; 20:1698–1700. [PubMed: 16807366]

Asikainen TM, Waleh NS, Schneider BK, Clyman RI, White CW. Enhancement of angiogenic effectors through hypoxia-inducible factor in preterm primate lung in vivo. Am J Physiol Lung Cell Mol Physiol. 2006b; 291:L588–95. [PubMed: 16679381]

Ban N, Matsumura Y, Sakai H, Takanezawa Y, Sasaki M, Arai H, Inagaki N. ABCA3 as a lipid transporter in pulmonary surfactant biogenesis. J Biol Chem. 2007; 282:9628–9634. [PubMed: 17267394]

Baraldi E, Filippone M. Chronic lung disease after premature birth. N Engl J Med. 2007; 357:1946–1955. [PubMed: 17989387]

Bekeredjian R, Walton CB, MacCannell KA, Ecker J, Kruse F, Outten JT, Sutcliffe D, Gerard RD, Bruick RK, Shohet RV. Conditional HIF-1alpha expression produces a reversible cardiomyopathy. PLoS One. 2010; 5:e11693. [PubMed: 20657781]

Bligh EG, Dyer WJ. A rapid method of total lipid extraction and purification. Can J Biochem Physiol. 1959; 37:911–917. [PubMed: 13671378]

Bridges JP, Ikegami M, Brilli LL, Chen X, Mason RJ, Shannon JM. LPCAT1 regulates surfactant phospholipid synthesis and is required for transitioning to air breathing in mice. J Clin Invest. 2010; 120:1736–1748. [PubMed: 20407208]

Bromley SK, Thomas SY, Luster AD. Chemokine receptor CCR7 guides T cell exit from peripheral tissues and entry into afferent lymphatics. Nat Immunol. 2005; 6:895–901. [PubMed: 16116469]

Bruick RK, McKnight SL. A conserved family of prolyl-4-hydroxylases that modify HIF. Science. 2001; 294:1337–1340. [PubMed: 11598268]

Cesarone CF, Bolognesi C, Santi L. Improved microfluorometric DNA determination in biological material using 33258 Hoechst. Anal Biochem. 1979; 100:188–197. [PubMed: 94515]

Chandel NS. Mitochondrial regulation of oxygen sensing. Adv Exp Med Biol. 2010; 661:339–354. [PubMed: 20204741]

Clark JC, Wert SE, Bachurski CJ, Stahlman MT, Stripp BR, Weaver TE, Whitsett JA. Targeted disruption of the surfactant protein B gene disrupts surfactant homeostasis, causing respiratory failure in newborn mice. Proc Natl Acad Sci USA. 1995; 92:7794–7798. [PubMed: 7644495]

Compernolle V, Brusselmans K, Acker T, Hoet P, Tjwa M, Beck H, Plaisance S, Dor Y, Keshet E, Lupu F, Nemery B, Dewerchin M, Van Veldhoven P, Plate K, Moons L, Collen D, Carmeliet P. Loss of HIF-2alpha and inhibition of VEGF impair fetal lung maturation, whereas treatment with VEGF prevents fatal respiratory distress in premature mice. Nat Med. 2002; 8:702–710. [PubMed: 12053176]

Del Monte G, Grego-Bessa J, Gonzalez-Rajal A, Bolos V, De La Pompa JL. Monitoring Notch1 activity in development: evidence for a feedback regulatory loop. Dev Dyn. 2007; 236:2594–2614. [PubMed: 17685488]

del Moral PM, De Langhe SP, Sala FG, Veltmaat JM, Tefft D, Wang K, Warburton D, Bellusci S. Differential role of FGF9 on epithelium and mesenchyme in mouse embryonic lung. Dev Biol. 2006; 293:77–89. [PubMed: 16494859]

Dioum EM, Clarke SL, Ding K, Repa JJ, Garcia JA. HIF-2alpha-haploinsufficient mice have blunted retinal neovascularization due to impaired expression of a proangiogenic gene battery. Invest Ophthalmol Vis Sci. 2008; 49:2714–2720. [PubMed: 18281611]

El-Chemaly S, Malide D, Zudaire E, Ikeda Y, Weinberg BA, Pacheco-Rodriguez G, Rosas IO, Aparicio M, Ren P, MacDonald SD, Wu HP, Nathan SD, Cuttitta F, McCoy JP, Gochuico BR, Moss J. Abnormal lymphangiogenesis in idiopathic pulmonary fibrosis with insights into cellular and molecular mechanisms. Proc Natl Acad Sci U S A. 2009; 106:3958–3963. [PubMed: 19237567]

Elson DA, Thurston G, Huang LE, Ginzinger DG, McDonald DM, Johnson RS, Arbeit JM. Induction of hypervascularity without leakage or inflammation in transgenic mice overexpressing hypoxia-inducible factor-1alpha. Genes Dev. 2001; 15:2520–2532. [PubMed: 11581158]

Ema M, Hirota K, Mimura J, Abe H, Yodoi J, Sogawa K, Poellinger L, Fujii-Kuriyama Y. Molecular mechanisms of transcription activation by HLF and HIF1alpha in response to hypoxia: their stabilization and redox signal-induced interaction with CBP/p300. EMBO J. 1999; 18:1905–1914. [PubMed: 10202154]

Epstein AC, Gleadle JM, McNeill LA, Hewitson KS, O'Rourke J, Mole DR, Mukherji M, Metzen E, Wilson MI, Dhanda A, Tian YM, Masson N, Hamilton DL, Jaakkola P, Barstead R, Hodgkin J, Maxwell PH, Pugh CW, Schofield CJ, Ratcliffe PJ. C. elegans EGL-9 and mammalian homologs

define a family of dioxygenases that regulate HIF by prolyl hydroxylation. Cell. 2001; 107:43–54. [PubMed: 11595184]

Fitzgerald ML, Xavier R, Haley KJ, Welti R, Goss JL, Brown CE, Zhuang DZ, Bell SA, Lu N, McKee M, Seed B, Freeman MW. ABCA3 inactivation in mice causes respiratory failure, loss of pulmonary surfactant, and depletion of lung phosphatidylglycerol. J Lipid Res. 2007; 48:621–632. [PubMed: 17142808]

Fukuda R, Zhang H, Kim JW, Shimoda L, Dang CV, Semenza GL. HIF-1 regulates cytochrome oxidase subunits to optimize efficiency of respiration in hypoxic cells. Cell. 2007; 129:111–122. [PubMed: 17418790]

Gao Y, Raj JU. Regulation of the pulmonary circulation in the fetus and newborn. Physiol Rev. 2010; 90:1291–1335. [PubMed: 20959617]

Gardner LB, Li Q, Park MS, Flanagan WM, Semenza GL, Dang CV. Hypoxia inhibits G1/S transition through regulation of p27 expression. J Biol Chem. 2001; 276:7919–7926. [PubMed: 11112789]

Gassmann M, Kvietikova I, Rolfs A, Wenger RH. Oxygen- and dioxin-regulated gene expression in mouse hepatoma cells. Kidney Int. 1997; 51:567–574. [PubMed: 9027741]

Gebb SA, Fox K, Vaughn J, McKean D, Jones PL. Fetal oxygen tension promotes tenascin-C-dependent lung branching morphogenesis. Dev Dyn. 2005; 234:1–10. [PubMed: 16086306]

Gebb SA, Jones PL. Hypoxia and lung branching morphogenesis. Adv Exp Med Biol. 2003; 543:117–125. [PubMed: 14713117]

Goda N, Ryan HE, Khadivi B, McNulty W, Rickert RC, Johnson RS. Hypoxia-inducible factor 1alpha is essential for cell cycle arrest during hypoxia. Mol Cell Biol. 2003; 23:359–369. [PubMed: 12482987]

Gossen M, Bujard H. Tight control of gene expression in mammalian cells by tetracycline-responsive promoters. Proc Natl Acad Sci U S A. 1992; 89:5547–5551. [PubMed: 1319065]

Green SL, Freiberg RA, Giaccia AJ. p21(Cip1) and p27(Kip1) regulate cell cycle reentry after hypoxic stress but are not necessary for hypoxia-induced arrest. Mol Cell Biol. 2001; 21:1196–1206. [PubMed: 11158306]

Groenman F, Rutter M, Caniggia I, Tibboel D, Post M. Hypoxia-inducible factors in the first trimester human lung. J Histochem Cytochem. 2007; 55:355–363. [PubMed: 17189520]

Grover TR, Asikainen TM, Kinsella JP, Abman SH, White CW. Hypoxia-inducible factors HIF-1alpha and HIF-2alpha are decreased in an experimental model of severe respiratory distress syndrome in preterm lambs. Am J Physiol Lung Cell Mol Physiol. 2007; 292:L1345–51. [PubMed: 17307811]

Gustafsson MV, Zheng X, Pereira T, Gradin K, Jin S, Lundkvist J, Ruas JL, Poellinger L, Lendahl U, Bondesson M. Hypoxia requires notch signaling to maintain the undifferentiated cell state. Dev Cell. 2005; 9:617–628. [PubMed: 16256737]

Hammel M, Michel G, Hoefer C, Klaften M, Muller-Hocker J, de Angelis MH, Holzinger A. Targeted inactivation of the murine Abca3 gene leads to respiratory failure in newborns with defective lamellar bodies. Biochem Biophys Res Commun. 2007; 359:947–951. [PubMed: 17577581]

Hassid WZ, Abraham S. Chemical procedures for analysis of polysaccharides. Methods Enzymol. 1957; 3:35–36.

Hogan BL, Yingling JM. Epithelial/mesenchymal interactions and branching morphogenesis of the lung. Curr Opin Genet Dev. 1998; 8:481–486. [PubMed: 9729726]

Huang LE, Gu J, Schau M, Bunn HF. Regulation of hypoxia-inducible factor 1alpha is mediated by an O2-dependent degradation domain via the ubiquitin-proteasome pathway. Proc Natl Acad Sci U S A. 1998; 95:7987–7992. [PubMed: 9653127]

Hyatt BA, Shangguan X, Shannon JM. BMP4 modulates fibroblast growth factor-mediated induction of proximal and distal lung differentiation in mouse embryonic tracheal epithelium in mesenchyme-free culture. Dev Dyn. 2002; 225:153–165. [PubMed: 12242715]

Ivan M, Haberberger T, Gervasi DC, Michelson KS, Gunzler V, Kondo K, Yang H, Sorokina I, Conaway RC, Conaway JW, Kaelin WGJ. Biochemical purification and pharmacological inhibition of a mammalian prolyl hydroxylase acting on hypoxia-inducible factor. Proc Natl Acad Sci U S A. 2002; 99:13459–13464. [PubMed: 12351678]

Iyer NV, Kotch LE, Agani F, Leung SW, Laughner E, Wenger RH, Gassmann M, Gearhart JD, Lawler AM, Yu AY, Semenza GL. Cellular and developmental control of O2 homeostasis by hypoxia-inducible factor 1 alpha. Genes Dev. 1998; 12:149–162. [PubMed: 9436976]

Kaner RJ, Ladetto JV, Singh R, Fukuda N, Matthay MA, Crystal RG. Lung overexpression of the vascular endothelial growth factor gene induces pulmonary edema. Am J Respir Cell Mol Biol. 2000; 22:657–664. [PubMed: 10837361]

Karkkainen MJ, Haiko P, Sainio K, Partanen J, Taipale J, Petrova TV, Jeltsch M, Jackson DG, Talikka M, Rauvala H, Betsholtz C, Alitalo K. Vascular endothelial growth factor C is required for sprouting of the first lymphatic vessels from embryonic veins. Nat Immunol. 2004; 5:74–80. [PubMed: 14634646]

Koritzinsky M, Magagnin MG, van den Beucken T, Seigneuric R, Savelkouls K, Dostie J, Pyronnet S, Kaufman RJ, Weppler SA, Voncken JW, Lambin P, Koumenis C, Sonenberg N, Wouters BG. Gene expression during acute and prolonged hypoxia is regulated by distinct mechanisms of translational control. EMBO J. 2006; 25:1114–1125. [PubMed: 16467844]

Koshiji M, Kageyama Y, Pete EA, Horikawa I, Barrett JC, Huang LE. HIF-1alpha induces cell cycle arrest by functionally counteracting Myc. EMBO J. 2004; 23:1949–1956. [PubMed: 15071503]

Lando D, Peet DJ, Gorman JJ, Whelan DA, Whitelaw ML, Bruick RK. FIH-1 is an asparaginyl hydroxylase enzyme that regulates the transcriptional activity of hypoxia-inducible factor. Genes Dev. 2002a; 16:1466–1471. [PubMed: 12080085]

Lando D, Peet DJ, Whelan DA, Gorman JJ, Whitelaw ML. Asparagine hydroxylation of the HIF transactivation domain a hypoxic switch. Science. 2002b; 295:858–861. [PubMed: 11823643]

Le Cras TD, Spitzmiller RE, Albertine KH, Greenberg JM, Whitsett JA, Akeson AL. VEGF causes pulmonary hemorrhage, hemosiderosis, and air space enlargement in neonatal mice. Am J Physiol Lung Cell Mol Physiol. 2004; 287:L134–42. [PubMed: 15033636]

Lee YM, Jeong CH, Koo SY, Son MJ, Song HS, Bae SK, Raleigh JA, Chung HY, Yoo MA, Kim KW. Determination of hypoxic region by hypoxia marker in developing mouse embryos in vivo: a possible signal for vessel development. Dev Dyn. 2001; 220:175–186. [PubMed: 11169851]

Li Y, Zhang H, Xie M, Hu M, Ge S, Yang D, Wan Y, Yan B. Abundant expression of Dec1/stra13/sharp2 in colon carcinoma: its antagonizing role in serum deprivation-induced apoptosis and selective inhibition of procaspase activation. Biochem J. 2002; 367:413–422. [PubMed: 12119049]

Lohela M, Helotera H, Haiko P, Dumont DJ, Alitalo K. Transgenic induction of vascular endothelial growth factor-C is strongly angiogenic in mouse embryos but leads to persistent lymphatic hyperplasia in adult tissues. Am J Pathol. 2008; 173:1891–1901. [PubMed: 18988807]

Mahon PC, Hirota K, Semenza GL. FIH-1: a novel protein that interacts with HIF-1alpha and VHL to mediate repression of HIF-1 transcriptional activity. Genes Dev. 2001; 15:2675–2686. [PubMed: 11641274]

Mallory BP, Mead TJ, Wiginton DA, Kulkarni RM, Greenberg JM, Akeson AL. Lymphangiogenesis in the developing lung promoted by VEGF-A. Microvasc Res. 2006; 72:62–73. [PubMed: 16806288]

Maltepe E, Schmidt JV, Baunoch D, Bradfield CA, Simon MC. Abnormal angiogenesis and responses to glucose and oxygen deprivation in mice lacking the protein ARNT. Nature. 1997; 386:403–407. [PubMed: 9121557]

Mason RJ, Nellenbogen J, Clements JA. Isolation of disaturated phosphatidylcholine with osmium tetroxide. J Lipid Res. 1976; 17:281–284. [PubMed: 932560]

Moens CB, Auerbach AB, Conlon RA, Joyner AL, Rossant J. A targeted mutation reveals a role for N-myc in branching morphogenesis in the embryonic mouse lung. Genes Dev. 1992; 6:691–704. [PubMed: 1577267]

Moens CB, Stanton BR, Parada LF, Rossant J. Defects in heart and lung development in compound heterozygotes for two different targeted mutations at the N-myc locus. Development. 1993; 119:485–499. [PubMed: 8287798]

Morimoto M, Liu Z, Cheng HT, Winters N, Bader D, Kopan R. Canonical Notch signaling in the developing lung is required for determination of arterial smooth muscle cells and selection of Clara versus ciliated cell fate. J Cell Sci. 2010; 123:213–224. [PubMed: 20048339]

Mukhopadhyay D, Tsiokas L, Sukhatme VP. Wild-type p53 and v-Src exert opposing influences on human vascular endothelial growth factor gene expression. Cancer Res. 1995; 55:6161–6165. [PubMed: 8521408]

Okubo T, Knoepfler PS, Eisenman RN, Hogan BL. Nmyc plays an essential role during lung development as a dosage-sensitive regulator of progenitor cell proliferation and differentiation. Development. 2005; 132:1363–1374. [PubMed: 15716345]

Oladipupo SS, Hu S, Santeford AC, Yao J, Kovalski JR, Shohet RV, Maslov K, Wang LV, Arbeit JM. Conditional HIF-1 induction produces multistage neovascularization with stage-specific sensitivity to VEGFR inhibitors and myeloid cell independence. Blood. 2011; 117:4142–4153. [PubMed: 21307392]

Perl AK, Zhang L, Whitsett JA. Conditional expression of genes in the respiratory epithelium in transgenic mice: cautionary notes and toward building a better mouse trap. Am J Respir Cell Mol Biol. 2009; 40:1–3. [PubMed: 19075182]

Rice WR, Conkright JJ, Na CL, Ikegami M, Shannon JM, Weaver TE. Maintenance of the mouse type II cell phenotype in vitro. Am J Physiol Lung Cell Mol Physiol. 2002; 283:L256–L264. [PubMed: 12114186]

Rocha SF, Adams RH. Molecular differentiation and specialization of vascular beds. Angiogenesis. 2009; 12:139–147. [PubMed: 19212819]

Ryan HE, Lo J, Johnson RS. HIF-1 alpha is required for solid tumor formation and embryonic vascularization. EMBO J. 1998; 17:3005–3015. [PubMed: 9606183]

Sahlgren C, Gustafsson MV, Jin S, Poellinger L, Lendahl U. Notch signaling mediates hypoxia-induced tumor cell migration and invasion. Proc Natl Acad Sci U S A. 2008; 105:6392–6397. [PubMed: 18427106]

Saini Y, Harkema JR, LaPres JJ. HIF1alpha is essential for normal intrauterine differentiation of alveolar epithelium and surfactant production in the newborn lung of mice. J Biol Chem. 2008; 283:33650–33657. [PubMed: 18801745]

Sawai S, Shimono A, Wakamatsu Y, Palmes C, Hanaoka K, Kondoh H. Defects of embryonic organogenesis resulting from targeted disruption of the N-myc gene in the mouse. Development. 1993; 117:1445–1455. [PubMed: 8404543]

Schlaeger TM, Bartunkova S, Lawitts JA, Teichmann G, Risau W, Deutsch U, Sato TN. Uniform vascular-endothelial-cell-specific gene expression in both embryonic and adult transgenic mice. Proc Natl Acad Sci U S A. 1997; 94:3058–3063. [PubMed: 9096345]

Schofield CJ, Ratcliffe PJ. Oxygen sensing by HIF hydroxylases. Nat Rev Mol Cell Biol. 2004; 5:343–354. [PubMed: 15122348]

Scortegagna M, Ding K, Oktay Y, Gaur A, Thurmond F, Yan LJ, Marck BT, Matsumoto AM, Shelton JM, Richardson JA, Bennett MJ, Garcia JA. Multiple organ pathology, metabolic abnormalities and impaired homeostasis of reactive oxygen species in Epas1−/− mice. Nat Genet. 2003; 35:331–340. [PubMed: 14608355]

Teles-Grilo ML, Leite-Almeida H, Martins dos Santos J, Oliveira C, Boaventura P, Grande NR. Differential expression of collagens type I and type IV in lymphangiogenesis during the angiogenic process associated with bleomycin-induced pulmonary fibrosis in rat. Lymphology. 2005; 38:130–135. [PubMed: 16353490]

Tzouvelekis A, Harokopos V, Paparountas T, Oikonomou N, Chatziioannou A, Vilaras G, Tsiambas E, Karameris A, Bouros D, Aidinis V. Comparative expression profiling in pulmonary fibrosis suggests a role of hypoxia-inducible factor-1alpha in disease pathogenesis. Am J Respir Crit Care Med. 2007; 176:1108–1119. [PubMed: 17761615]

van Tuyl M, Liu J, Wang J, Kuliszewski M, Tibboel D, Post M. Role of oxygen and vascular development in epithelial branching morphogenesis of the developing mouse lung. Am J Physiol Lung Cell Mol Physiol. 2005; 288:L167–78. [PubMed: 15377493]

Warburton D, Schwarz M, Tefft D, Flores-Delgado G, Anderson KD, Cardoso WV. The molecular basis of lung morphogenesis. Mech Dev. 2000; 92:55–81. [PubMed: 10704888]

Wenger RH, Stiehl DP, Camenisch G. Integration of oxygen signaling at the consensus HRE. Sci STKE. 2005:re12. [PubMed: 16234508]

White AC, Xu J, Yin Y, Smith C, Schmid G, Ornitz DM. FGF9 and SHH signaling coordinate lung growth and development through regulation of distinct mesenchymal domains. Development. 2006; 133:1507–1517. [PubMed: 16540513]

Yamashita T, Ohneda O, Nagano M, Iemitsu M, Makino Y, Tanaka H, Miyauchi T, Goto K, Ohneda K, Fujii-Kuriyama Y, Poellinger L, Yamamoto M. Abnormal heart development and lung remodeling in mice lacking the hypoxia-inducible factor-related basic helix-loop-helix PAS protein NEPAS. Mol Cell Biol. 2008; 28:1285–1297. [PubMed: 18070924]

Young RM, Wang SJ, Gordan JD, Ji X, Liebhaber SA, Simon MC. Hypoxia-mediated selective mRNA translation by an internal ribosome entry site-independent mechanism. J Biol Chem. 2008; 283:16309–16319. [PubMed: 18430730]

Yu AY, Frid MG, Shimoda LA, Wiener CM, Stenmark K, Semenza GL. Temporal, spatial, and oxygen-regulated expression of hypoxia-inducible factor-1 in the lung. Am J Physiol. 1998; 275:L818–26. [PubMed: 9755115]

Yun Z, Maecker HL, Johnson RS, Giaccia AJ. Inhibition of PPAR gamma 2 gene expression by the HIF-1-regulated gene DEC1/Stra13: a mechanism for regulation of adipogenesis by hypoxia. Dev Cell. 2002; 2:331–341. [PubMed: 11879638]

Zeng X, Wert SE, Federici R, Peters KG, Whitsett JA. VEGF enhances pulmonary vasculogenesis and disrupts lung morphogenesis in vivo. Develop Dynam. 1998; 211:215–227.

Zhang H, Bosch-Marce M, Shimoda LA, Tan YS, Baek JH, Wesley JB, Gonzalez FJ, Semenza GL. Mitochondrial autophagy is an HIF-1-dependent adaptive metabolic response to hypoxia. J Biol Chem. 2008; 283:10892–10903. [PubMed: 18281291]

Zhang H, Gao P, Fukuda R, Kumar G, Krishnamachary B, Zeller KI, Dang CV, Semenza GL. HIF-1 inhibits mitochondrial biogenesis and cellular respiration in VHL-deficient renal cell carcinoma by repression of C-MYC activity. Cancer Cell. 2007; 11:407–420. [PubMed: 17482131]

Highlights

- Conditional HIF1a expression in the fetal lung epithelium disrupts morphogenesis
- HIF1a induction inhibits proliferation and impairs maturation of epithelial cells
- HIF1a induces lymphangiogenesis in the developing lung

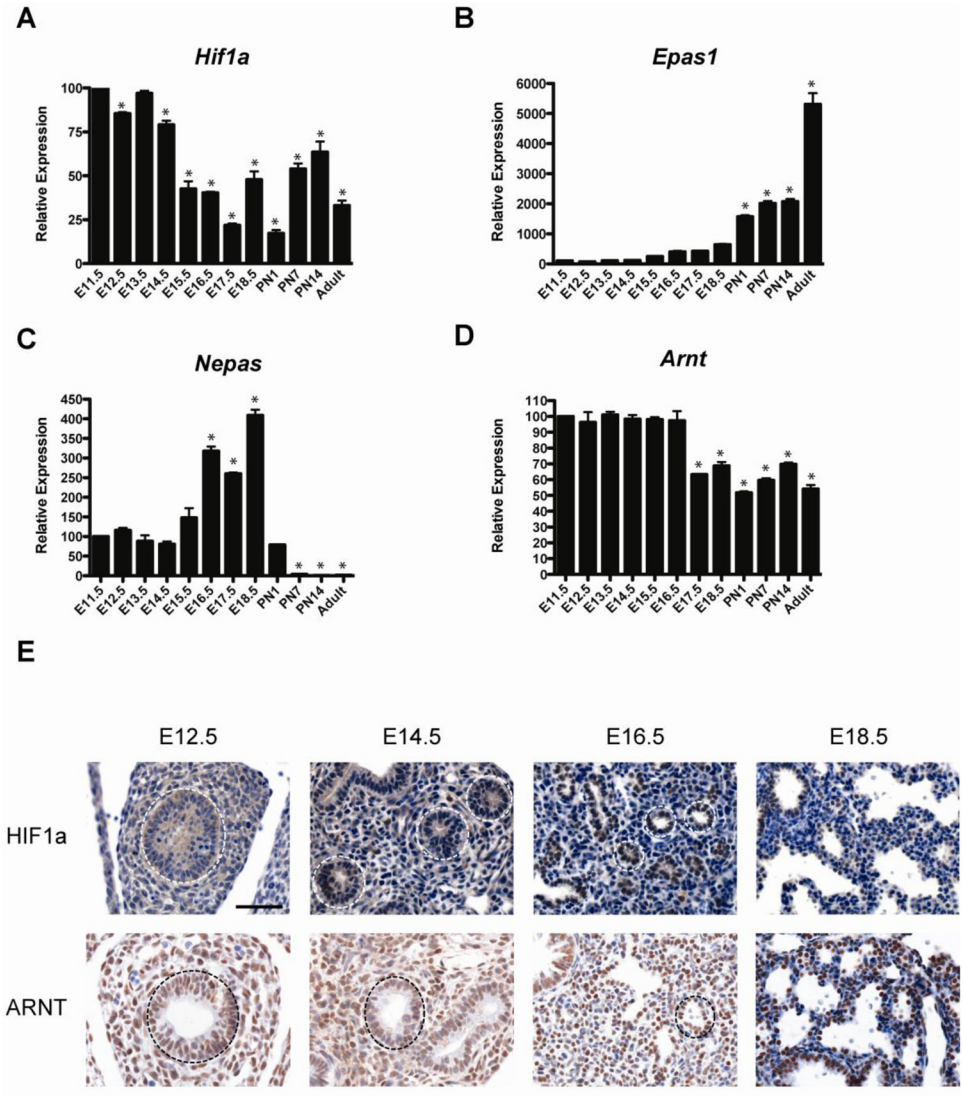

Figure 1.

Ontogeny of Hif1a, Epas1, Hif3a and Arnt in the developing mouse lung. A–D) qPCR of whole mouse lung for *Hif1a*, *Epas1*, Hif3a and *Arnt* from E11.5 to adult. Note differences in scale on the graphs for relative expression of the target genes. n=3 lungs per gestational age. *p<0.05 vs. E11.5. E) Immunostaining for HIF1a and ARNT in the developing lung. Note nuclear staining of HIF1a protein in the epithelial cells (white dotted circles) throughout gestation, with highest levels observed at E18.5. ARNT protein is detected in both mesenchymal and epithelial cells (black dotted circles) throughout gestation. Scale bar = 50μm.

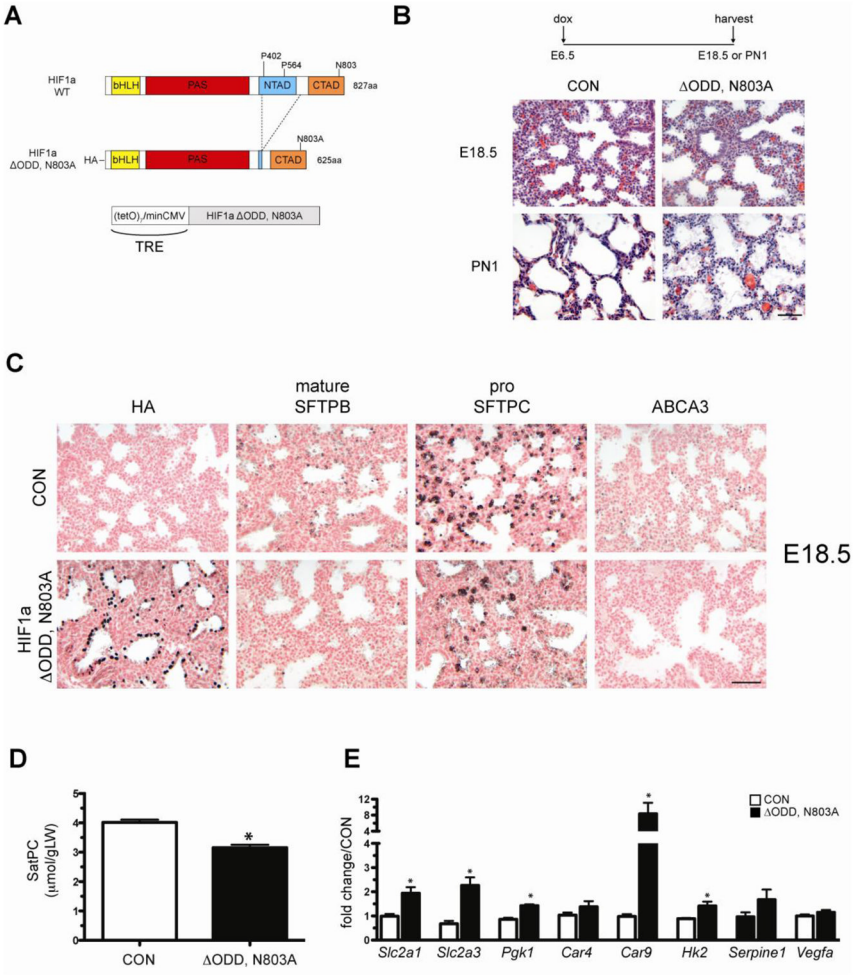

Figure 2.

Epithelial expression of HIF1a ΔODD,N803A during lung development results in perinatal lethality. A) Diagram of the HIF1a ΔODD,N803A transgene. The HIF1a ΔODD,N803A transgene was placed under the control of the tetracycline-responsive element (TRE) and transgenic animals were generated. B) H&E staining of lungs from single transgenic control animals (CON) or bi-transgenic *hSftpc*-rtTA/TRE HIF1a ΔODD,N803A (ΔODD,N803A) on dox from E6.5 until harvest at E18.5 or postnatal day 1 (PN1). Note normal morphology of ΔODD,N803A lungs at E18.5 and decreased mesenchymal thinning and airspace debris in ΔODD,N803A lungs at PN1 compared to controls. C) Immunohistochemical analyses of distal epithelial marker expression in CON and ΔODD,N803A animals at E18.5. Note the nuclear staining of the HA-tagged transgenic protein and the overall decrease of the surfactant-associated proteins, SFTPB, SFTPC and ABCA3, in ΔODD,N803A vs. CON lungs. D) Saturated phosphatidylcholine (SatPC) levels were slightly decreased in ΔODD,N803A lungs vs. CON at E18.5. n=6 samples per genotype. *p<0.05 vs. CON. E) Gene expression in E14.5 ΔODD,N803A and CON lungs. Note increased expression of the glucose transporters *Slc2a1* and *Slc2a3*, as well as *Pgk1*, *Car9* and *Hk2* in ΔODD,N803A lungs vs. CON. n=3–6 samples per genotype. *p<0.05 vs. CON.

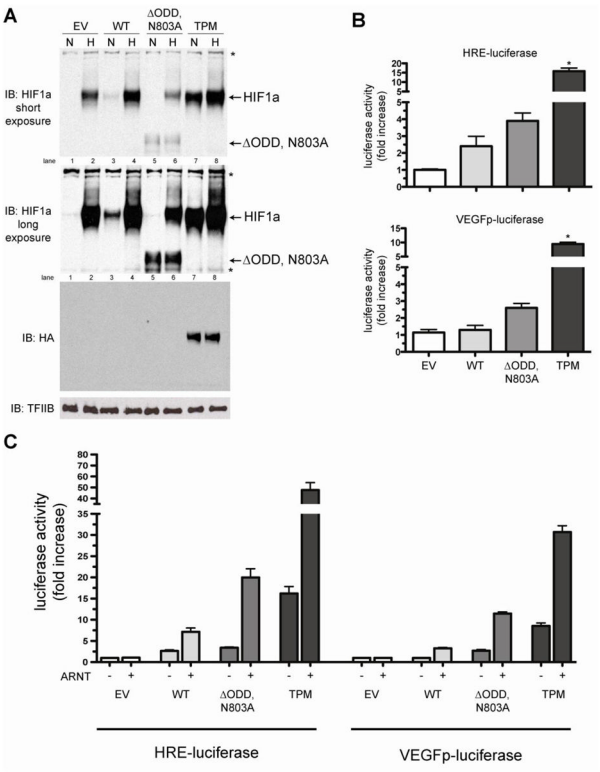

Figure 3.

Comparison of protein stability and transactivation potential of the HIF1a triple point mutant (TPM) vs. ΔODD,N803A. A) Immunoblot analyses of nuclear extracts from HeLa cells with anti-HIFa and anti-HA antibodies. Cells were transfected with empty vector (EV), HIF1a wild-type (WT), HIF1a ΔODD,N803A (ΔODD,N803A) or the HIF1a triple point mutant (TPM) for 24hrs, then exposed to either normoxia (N) or hypoxia (H; 1%O_2) for 17hrs. All HIF constructs contained a C-terminal HA tag. Note the increased stability of the TPM in normoxia compared to the WT and ΔODD,N803A constructs (lane 7 vs. lanes 3 and 5, HIF1a band), that expression of the TPM mutant is hypoxia-insensitive (compare lanes 7 and 8 in the HA blot) and that the ΔODD,N803A protein inhibits the hypoxic induction of endogenous HIF1a (lane 6 vs. 2, HIF1a band). *=non-specific bands. B) HIF1a TPM is a more potent inducer of two HIF-responsive promoters, HRE-luciferase and VEGFp-luciferase, than WT or ΔODD,N803A constructs in transfected HeLa cells. Data is compiled from 3 separate experiments, with 3 replicates per experiment. *$p<0.05$ vs. EV. C) Co-transfection of ARNT with the HIF1a constructs into HeLa cells potentiates the transactivation of HIF1a on two distinct HIF-responsive promoters, HRE-luc and VEGFp-luc. Data is compiled from 3 separate experiments, with 3 replicates per experiment.

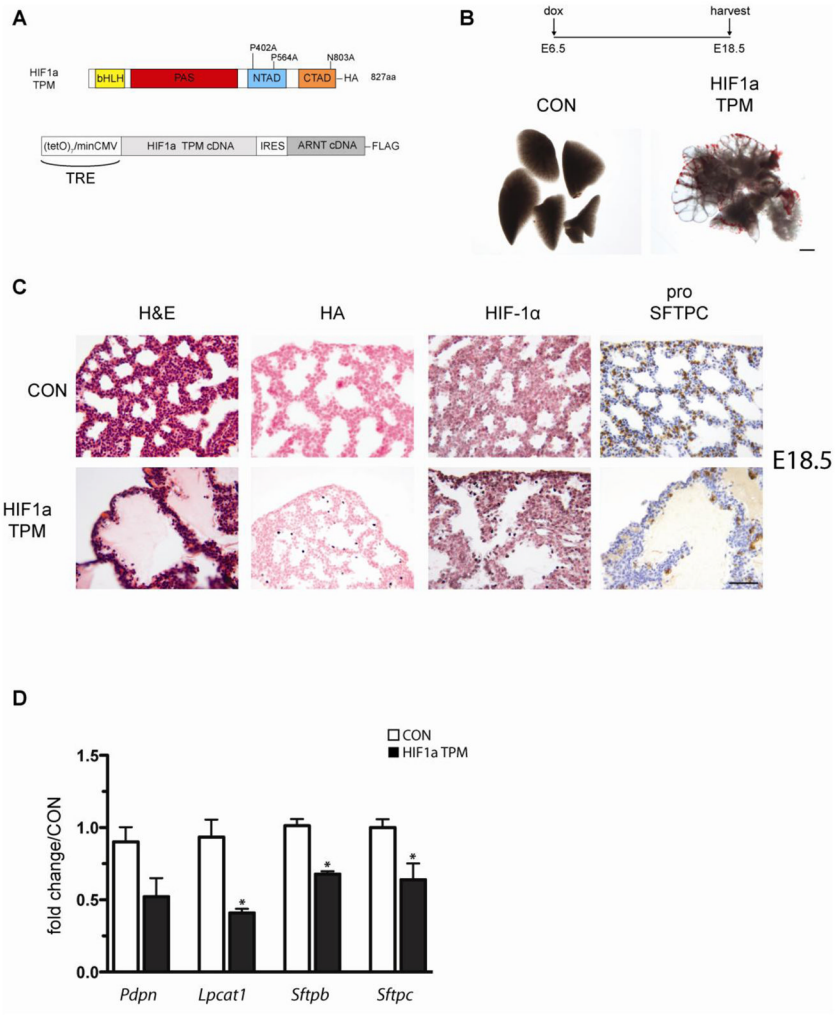

Figure 4.

Epithelial expression of HIF1a TPM during lung development perturbs lung morphogenesis. A) Diagram of the conditional HIF1a TPM–IRES–ARNT transgene. The HIF1a TPM–IRES–ARNT cassette was placed under the control of the tetracycline-responsive element (TRE) and transgenic animals were generated. B) Gross image views of lungs from single transgenic control animals (CON) or bi-transgenic *Sftpc*-rtTA/TRE HIF1a triple point mutant (TPM) animals on dox from E6.5 until harvest at E18.5. Note cystic morphology of lung parenchyma in TPM vs. CON animals. Scale bar = 500μm. C) H&E staining and immunohistochemistry of HIF1a TPM and CON lungs at E18.5. The distal airspaces of HIF1a TPM lungs were filled with proteinaceous debris and contained hypertrophic epithelial cells (H&E). Note the mosaic expression pattern of the HIF1a TPM transgene at this embryonic stage as detected with anti-HA and HIF1a antibodies. Also note decreased staining of the distal epithelial marker pro SFTPC in HIF1a TPM lungs vs. CON. Scale bar = 50μm. D) Decreased expression of distal epithelial markers in HIF1a TPM lungs. qPCR of distal lung markers in HIF1a TPM lungs vs. CON at E18.5. n=3–6 samples per genotype. *p<0.05 vs. CON.

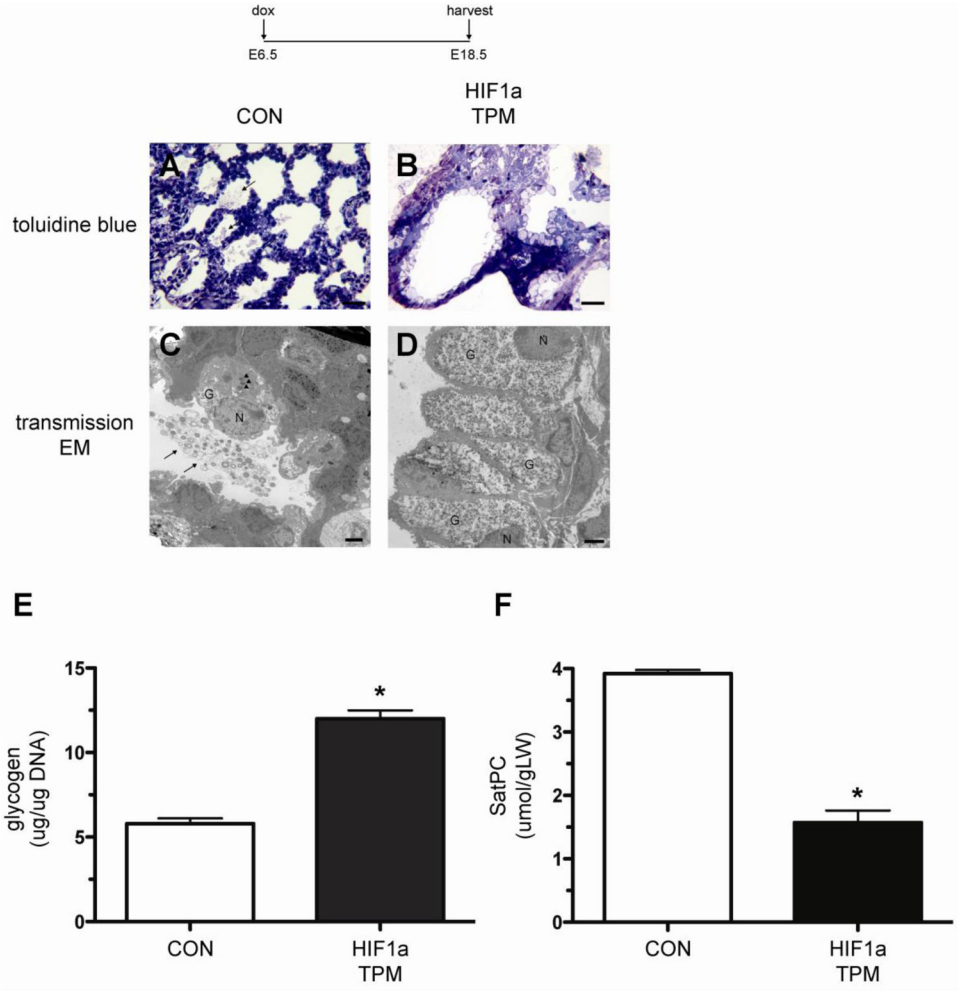

Figure 5.

Decreased maturation of distal epithelial cells in HIF1a TPM lungs at E18.5. A–D) Note abundant surfactant in airspaces of CON lungs (arrows, panels A and C) compared to absence of surfactant in HIF1a TPM lungs (panels B and D) in toluidine-stained sections and electron micrographs. Alveolar type II cells from CON lungs contained lamellar bodies (arrowheads, panel C) while the distal epithelium HIF1a TPM lungs were devoid of lamellar bodies and contained abundant glycogen stores (panel D vs. C). G = glycogen, N = nucleus. Scale bar = 30μm for panels A and B, 2μm for panels C and D. E) Glycogen assays demonstrate increased glycogen stores in HIF1a TPM lungs at E18.5 vs. CON. Total glycogen content was normalized to genomic DNA. n=6 samples per genotype. *p<0.05 vs. CON. F) Saturated phosphatidylcholine (SatPC) is significantly decreased in E18.5 HIF1a TPM lungs vs. CON. n=5 samples per genotype. *p<0.05 vs. CON.

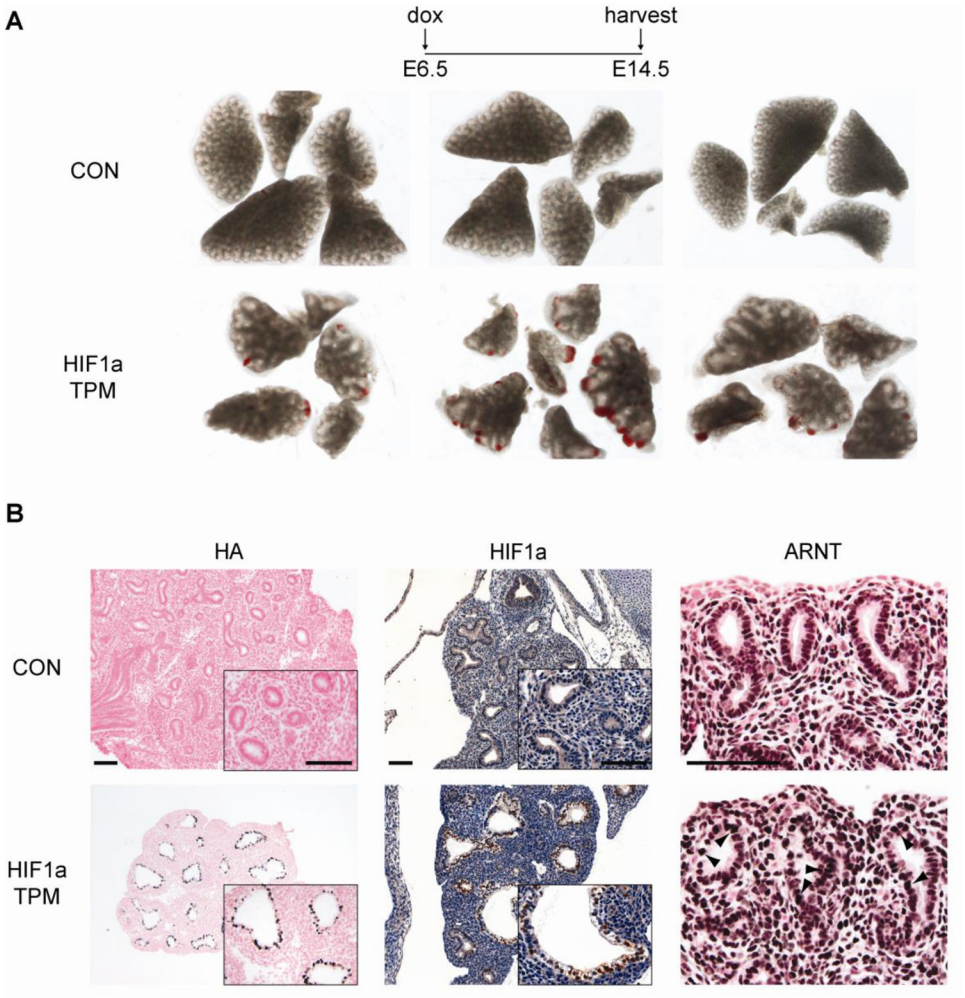

Figure 6.

Defective branching morphogenesis and hemorrhaging in HIF1a TPM lungs at E14.5. A) Gross views of lungs from individual CON and HIF1a TPM littermates on dox from E6.5 until harvest at E14.5. Note branching defects as evidenced by large cysts in distal airways, overall hypoplasia of lung tissue and subpleural hemorrhaging in HIF1a TPM lungs vs. CON. B) Immunostaining of HIF1a TPM lungs vs. CON at E14.5. The HIF1a TPM transgene is abundantly expressed in the distal lung epithelium of HIF1a TPM lungs as detected by anti-HA and anti-HIF1a antibodies. Note increased staining of ARNT in distal epithelial cells of HIF1a TPM lungs (arrowheads), indicating expression of the ARNT transgene. Scale bars = 100μm.

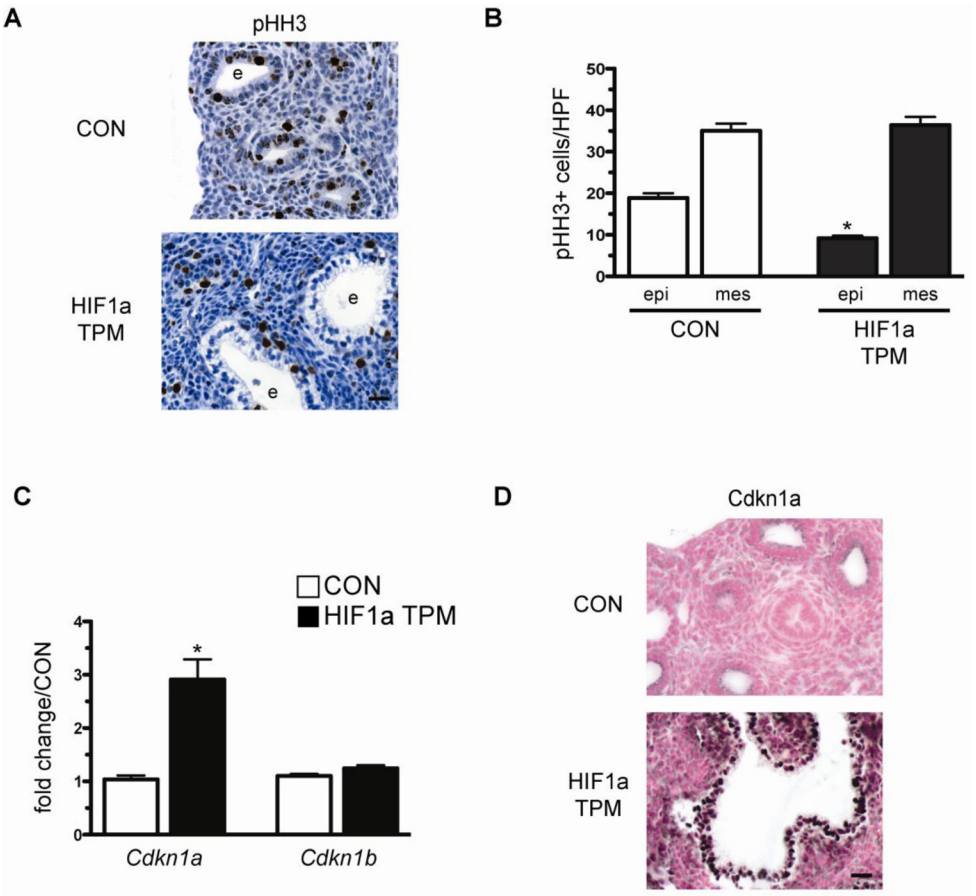

Figure 7.

Reduced cell proliferation and induction of Cdkn1a in HIF1a TPM epithelium at E14.5. A) Representative image of phospho-histone H3 (pHH3) immunostaining in a HIF1a TPM lung vs. CON. Note the decreased staining of pHH3 in the epithelium of HIF1a TPM lungs vs. CON. e = epithelium. Scale bar = 100μm. B) Quantitative analysis of pHH3 staining indicates decreased proliferation of the epithelium in HIF1a TPM lungs vs. CON. Note that mesenchymal proliferation did not differ between the two genotypes. *p<0.05 vs CON epi. epi = epithelium, mes = mesenchyme. C) qPCR analysis of Cdkn1a and Cdkn1b in HIF1a TPM and CON lungs at E14.5. n=5 samples per genotype. *p<0.05 vs CON. D) Representative image of Cdkn1a immunostaining in a HIF1a TPM lung vs. CON. Note increased staining of the epithelium of HIF1a TPM lungs vs. CON. e = epithelium. Scale bar = 100μm.

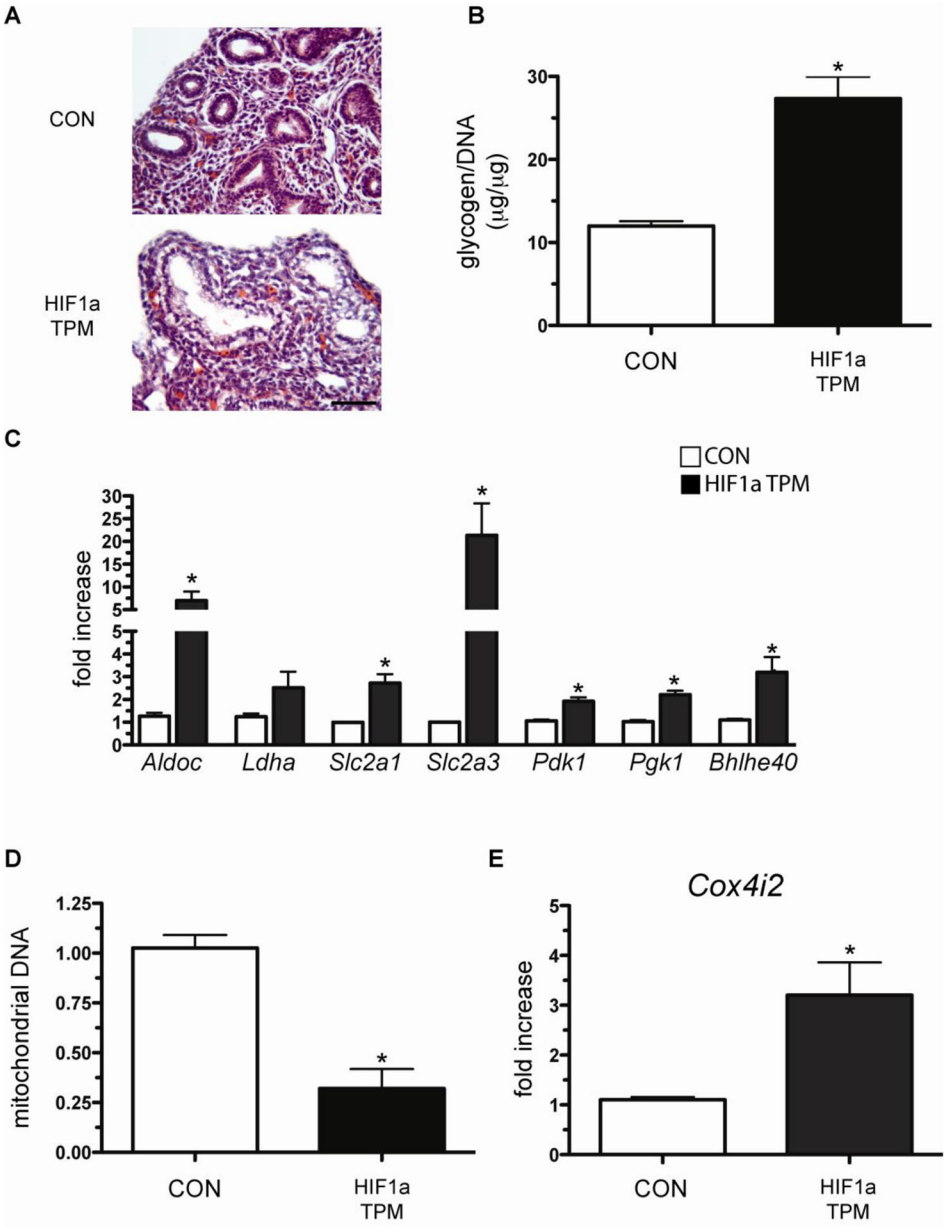

Figure 8.

Epithelial expression of HIF1a TPM induces a glycolytic switch in embryonic distal epithelial cells. A) H&E staining reveals cystic airways and hypertrophic epithelial cells in HIF1a TPM lungs on dox from E6.5 until harvest at E14.5. B) Glycogen assays demonstrate increased glycogen stores in HIF1a TPM lungs at E14.5 vs. CON. Total glycogen content was normalized to genomic DNA. n=3–6 samples per genotype. *p<0.05 vs. CON. C) HIF1a TPM lungs show increased transcriptional expression of glucose transporters (*Slc2a1*, *Slc2a3*), glycolytic enzymes (*Aldoc*, *Pdk1*, *Pgk1*) and a gene known to inhibit apoptosis and promote HIF1a-dependent repression of lipogenesis (*Bhlhe40*). n=3–6 samples per genotype. *p<0.05 vs. CON. D) Mitochondrial content from whole lung homogenates was decreased in HIF1a TPM lungs. n=4 samples per genotype. *p<0.05 vs. CON. E) qPCR

analysis indicating that HIF1a TPM lungs have increased expression of cytochrome c oxidase subunit IV isoform 2. n=6 samples per genotype. *p<0.05 vs. CON.

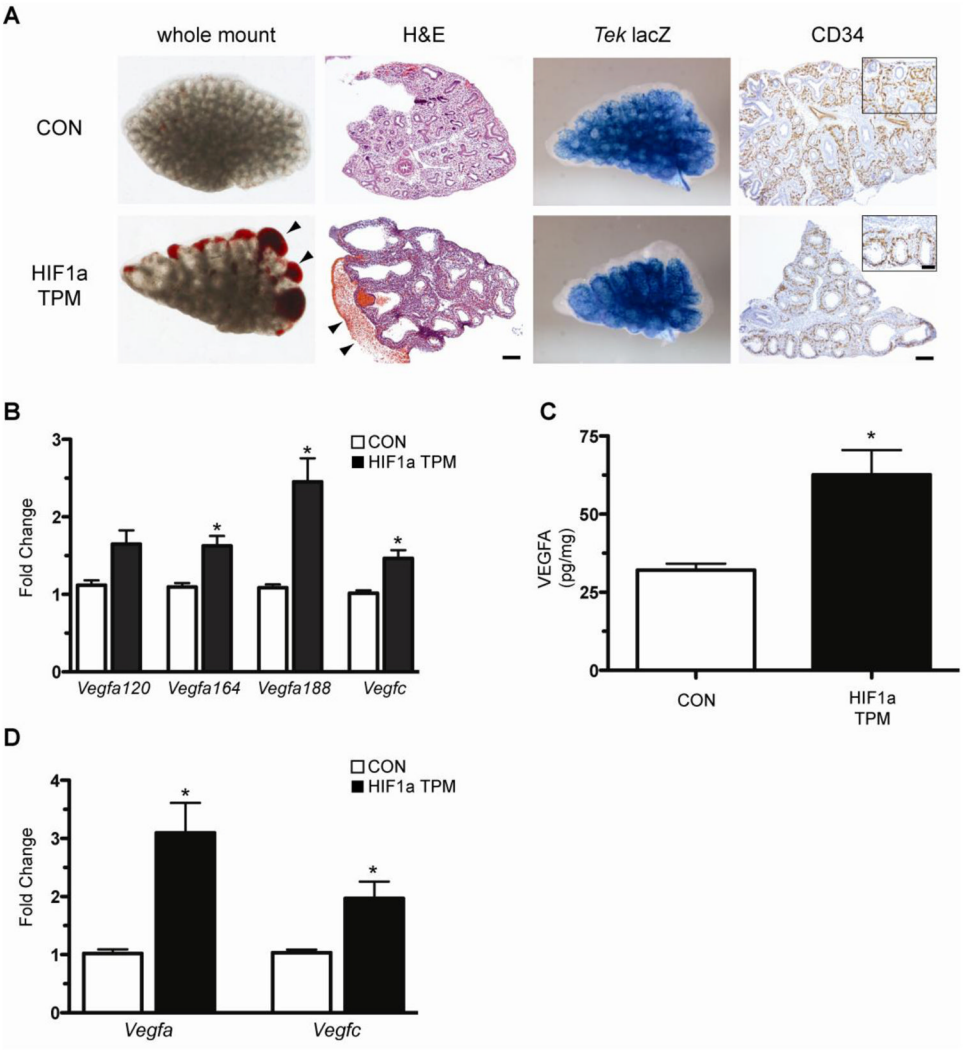

Figure 9.

Compromised vascular integrity in HIF1a TPM embryonic lungs. A) Whole mount images and H&E sections demonstrate sub-plural hemorrhaging (arrowheads) in the HIF1a TPM lungs that were administered dox from E6.5 until harvest at E14.5. Gross development of the vascular plexus was not perturbed as illustrated by whole mount β-galactosidase assays of *Tek*-LacZ/*Sftpc*- rtTA/*TRE*-HIF1a TPM triple transgenic lungs and sections stained with anti-CD34 antibody. Scale bars = 100μm for large images, 50μm for insets. B) qPCR analysis demonstrates increased expression of the *Vegfa* isoforms $Vegfa_{164}$ and $Vegfa_{188}$, and the *Vegfc* gene in HIF1a TPM lungs. n=3–6 samples per genotype. *p<0.05 vs. CON. C) VEGFA protein was significantly increased in HIF1a TPM whole lung homogenates compared to CON animals. n=6 samples per genotype. *p<0.05 vs. CON. D) *Vegfa and Vegfc* mRNA levels are increased in primary type II cells isolated from HIF1a TPM adult mice. Dox was administered in culture for 24hrs to induce expression of the HIF1a TPM transgene. n=4 samples per genotype. *p<0.05 for panels B–D.

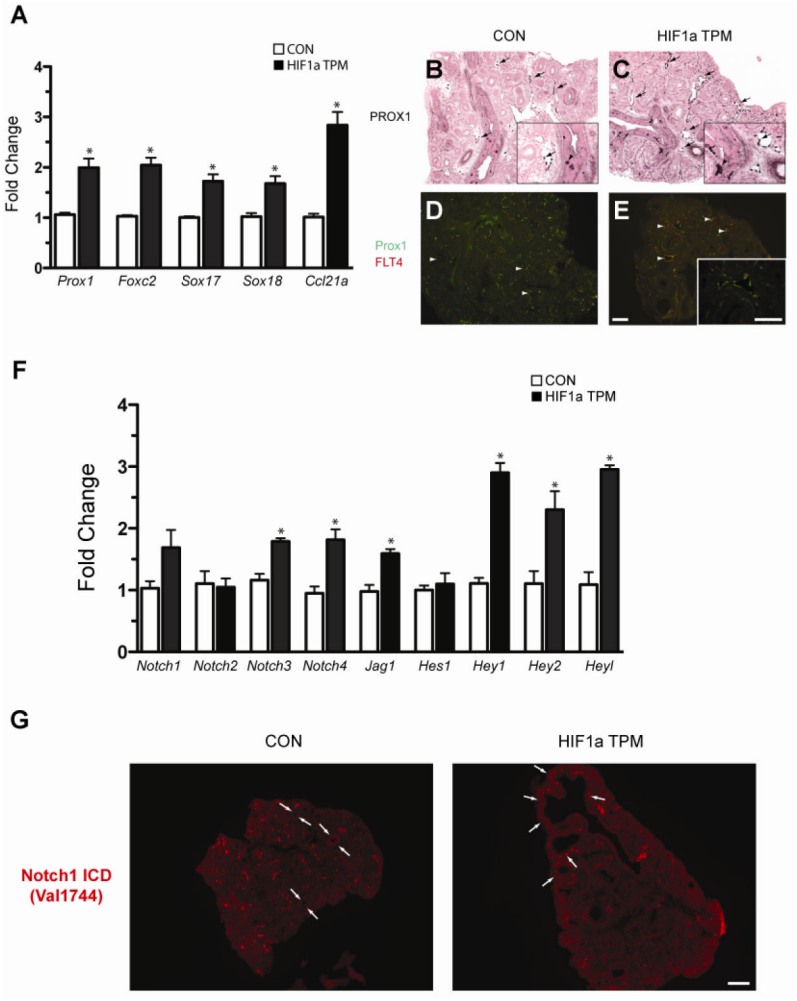

Figure 10.

Epithelial HIF1a TPM expression induces lymphangiogenesis in the embryonic lung. A) qPCR analysis of lymphangiogenic markers in HIF1a TPM lungs on dox from E6.5 until harvest at E14.5. n=3–5 samples per genotype. *p<0.05 vs. CON. B–E) PROX-1 immunostaining in E14.5 lungs. Note increased numbers of PROX1+ endothelial cells in lymphatic vessels of HIF1a TPM lungs (C vs. B, arrows) and PROX1+ staining in neuroendocrine cells of the epithelium (B and C, arrowheads). An increase in the number and size of PROX1+/FLT4+ lymphatic vessels was also observed in HIF1a TPM lungs compared to CON (panels D and E, arrowheads). Scale bars = 100μm. F) qPCR analyses demonstrates increased expression of the Notch signaling pathway genes in HIF1a TPM lungs. n=3–6 samples per genotype. *p<0.05 vs. CON. G) Notch1 signaling is increased in the mesenchyme subtending the proximal epithelium of HIF1a TPM lungs (arrows), as demonstrated by immunofluorescent staining with the cleaved Notch1 antibody Val1744. Scale bars = 200μm.

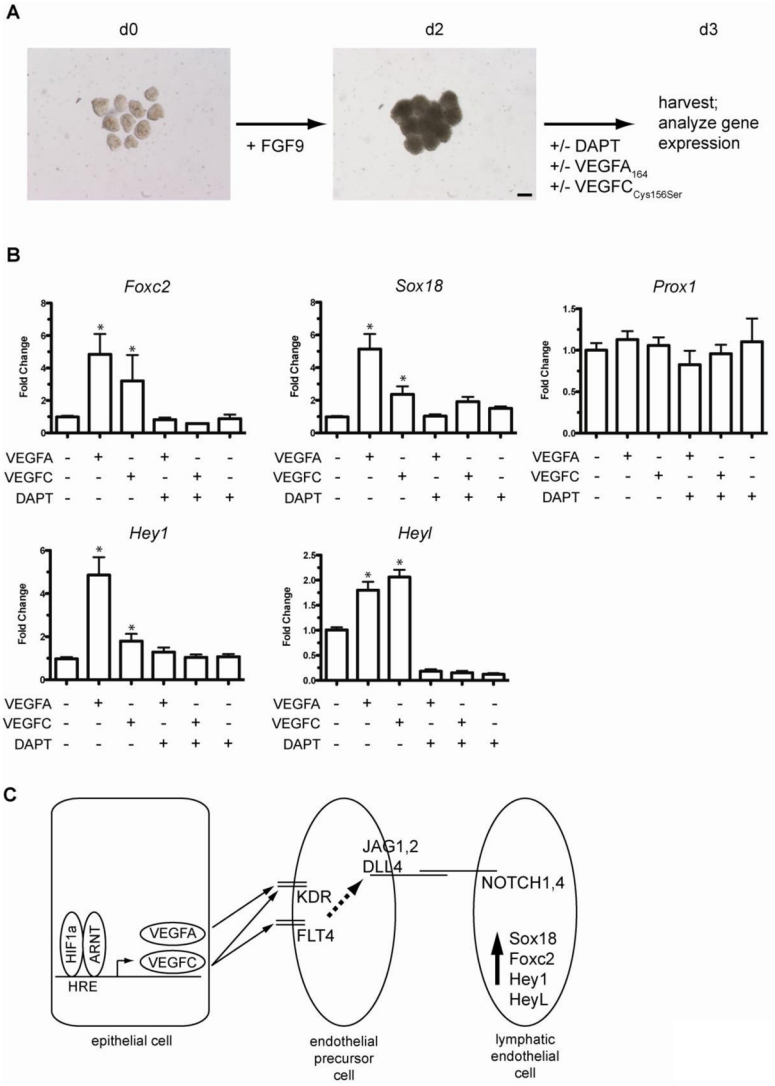

Figure 11.

VEGFA and VEGFC are sufficient to induce Notch-dependent activation of lymphangiogenic markers in fetal lung mesenchyme. A) Diagram outlining the experimental protocol. Lung mesenchyme was isolated from E12.5 mice on d0, treated as indicated and analyzed at d3. Scale bar = 100μm. B) qPCR analysis of fetal lung mesenchyme on d3 following treatment with VEGFA-165, VEGFC and/or treatment with the Notch pathway inhibitor DAPT. Note that both VEGFA and VEGFC recombinant proteins were sufficient to induce *Foxc2*, *Hey1*, *Heyl and Sox18* and that this induction was inhibited by co-treatment with the Notch inhibitor DAPT. Data are compiled from 3 separate experiments, with 3 samples per group in each experiment. *p<0.05 vs. untreated mesenchyme control. C) Model of epithelial HIF1a induction of VEGFA and VEGFC and the downstream activation of lymphangiogenic markers on endothelial cell precursors in the fetal lung mesenchyme.